March 1986 LS-51

6 GeV Synchrotron X-Ray Source Conceptual Design Report

Supplement B

Conceptual Design of Proposed Beam Lines for the 6 GeV Light Source

Argonne National Laboratory, Argonne, Illinois 60439
operated by The University of Chicago for the U. S. Department of Energy under Contract W-31-109-Eng-38

DISCLAIMER

SUPPLEMENT B

CONCEPTUAL DESIGN OF PROPOSED BEAMLINES

FOR THE 6 GeV LIGHT SOURCE

TABLE OF CONTENTS

TABLE OF CONTENTS (Cont'd)

Page

TABLE OF CONTENTS (Cont'd)

LIST OF FIGURES

LIST OF FIGURES (Cont'd)

LIST OF TABLES

1 Introduction

In this document, preliminary conceptual designs are presented for ten sample beamlines for the 6 GeV Light Source. These beamlines will accommodate investigations in solid-state physics, materials science, materials technology, chemical technology, and biological and medical sciences. In future, the designs will be altered to include new developments in x-ray optics and hardware technologies. The research areas addressed by the samples beamlines are as follows:

- Topography and Radiography/Tomography (Section 2)
- Inelastic Scattering with Ultrahigh Energy Resolution (Section 3)
- Surface and Bulk Studies Using High Momentum Resolution (Section 4)
- Inelastic Scattering from Charge and Spin (Section 5)
- Advanced X-Ray Photoelectron Spectroscopy Studies (Section 6)
- Small Angle X-Ray Scattering Studies (Section 7)
- General Purpose Scattering for Materials Studies (Section 8)
- Multiple-Energy Anomalous-Dispersion Studies of Proteins (Section 9)
- Protein Crystallography (Section 10)
- Time- and Space-resolved X-Ray Spectroscopy (Section 11)
- Medical Diagnostic Facility (Section 12)
- Transuranium Research Facility (Section 13)

The computer systems to be used on the beamlines are also discussed in Section 14 of this document.

2 Topography and Radiography/Tomography

2.1 Introduction

High-intensity synchrotron radiation sources provide a range of modern material characterization techniques (mostly nondestructive) for investigating a variety of problems related to defects in solids. These techniques include x-ray diffraction topography, differential-absorption radiography, and transmission and fluorescence tomography. A beamline is proposed which takes advantage of the unique features of 6 GeV synchrotron radiation to create a state-of-the-art facility for applying these techniques. The proposed beamline is designed to utilize both monochromatic and white-beam radiation. By building a composite wiggler line with these combined capabilities, one can realize considerable cost savings [e.g., by elimination of a separate insertion device (ID)]. Furthermore, the beamline will permit more quantitative analysis of the information derived from tomography and plane-wave topography than is presently possible. The high brightness and energy tunability of radiation from the proposed machine will produce an unparalleled capability for real-time characterization with the above-mentioned techniques. Wide area coverage of the sample by the x-ray beam is essential for real-time work and is beyond the capabilities of existing U.S. machines. Exposure times on the proposed beamline will be as much as 7000 times shorter than those required at existing facilities. Also, this beamline will allow examination of flaws in "bulk" environments, which is critical to our understanding of the mechanical properties of materials.

The specific types of investigations that will be possible include the following: (1) Crack initiation and propagation studies in advanced high-temperature materials; (2) in-situ observations of thin-film processing; (3) analysis of elastic wave propagation in solids; (4) three-dimensional

imaging of flaws and distribution of elements in high-temperature materials; (5) studies of dislocation dynamics in thick sections, leading to a better understanding of crack nucleation; (6) precipitation studies in alloys; (7) assessment of crystal growth for control of microstructures in electronic devices; and (8) observation of flaws on surfaces and in interfaces.

2.2 Beamline Performance Parameters

In designing a beamline for state-of-the-art x-ray imaging, it is critical to take into account three parameters: (a) geometric resolution; (b) the area covered by the x-ray beam in illuminating the sample; and (c) the intensity delivered to the sample and that available to diffraction or radiography detectors. The implications of these parameters were discussed at a recent workshop,[1] and the following conclusions were reached: First, the geometric resolution should be at least of the order of 1 μm, especially with the new photolithographic copolymers. Since the potential detector resolution may be as high as 0.1 μm, this should be feasible. Second, the area coverage is extremely important, for if the sample is not fully illuminated, the detection of real-time events becomes virtually impossible, since one cannot predict where in the specimen they will occur. Third, the intensity should be significantly higher than in currently operating synchrotrons to permit real-time measurements of dynamic events. The geometric resolution, area coverage, and intensity of the proposed beamline at the two planned experimental stations are evaluated in Section 2.3 below.

2.3 Beamline Design

One way to achieve both high intensity and wide area coverage is to build two separate beamlines, one very long for wide area coverage and one close to the source for high-intensity illumination. Alternatively, one can build a single long line with a "side" station located closer to the source. Unfortunately, side-station designs often introduce optical elements which can severely degrade image quality. Instead, the approach we have chosen for the beamline layout for the topography and radiography/tomography facility is to split the beam aperture in the horizontal plane at ~70 m from the source. The divided aperture will divert half of the beam to a monochromator and into a hutch (Station 1) with a monochromatic x-ray camera and associated facilities located at about 2 m above the original beam axis. The other half of the beam will be piped through the Station 1 hutch and out of the 6 GeV facility to a separate building located at ~350 m downstream (Station 2), which will house the monochromatic plane-wave and white-beam cameras. A schematic drawing of this setup is shown in Fig. 2-1.

The key component at Station 1 is a double-crystal monochromator with plug-in crystal optics, which can be used in either the symmetric or asymmetric mode (depending on the experiment) to deliver high-intensity illumination to the camera in Station 1. Adjacent to this hutch will be a control room and a small darkroom for film processing. The portion of the beam that is delivered to Station 2 will impinge on a monochromator, which will divert the beam to an optical bench and eventually to the plane-wave topography camera situated at 90° to the beamline optical axis. The monochromator can be taken out of the optical system so that the white radiation will impinge on a white-beam camera at the 350 m position. This arrangement will provide wide-area sample illumination with reasonable

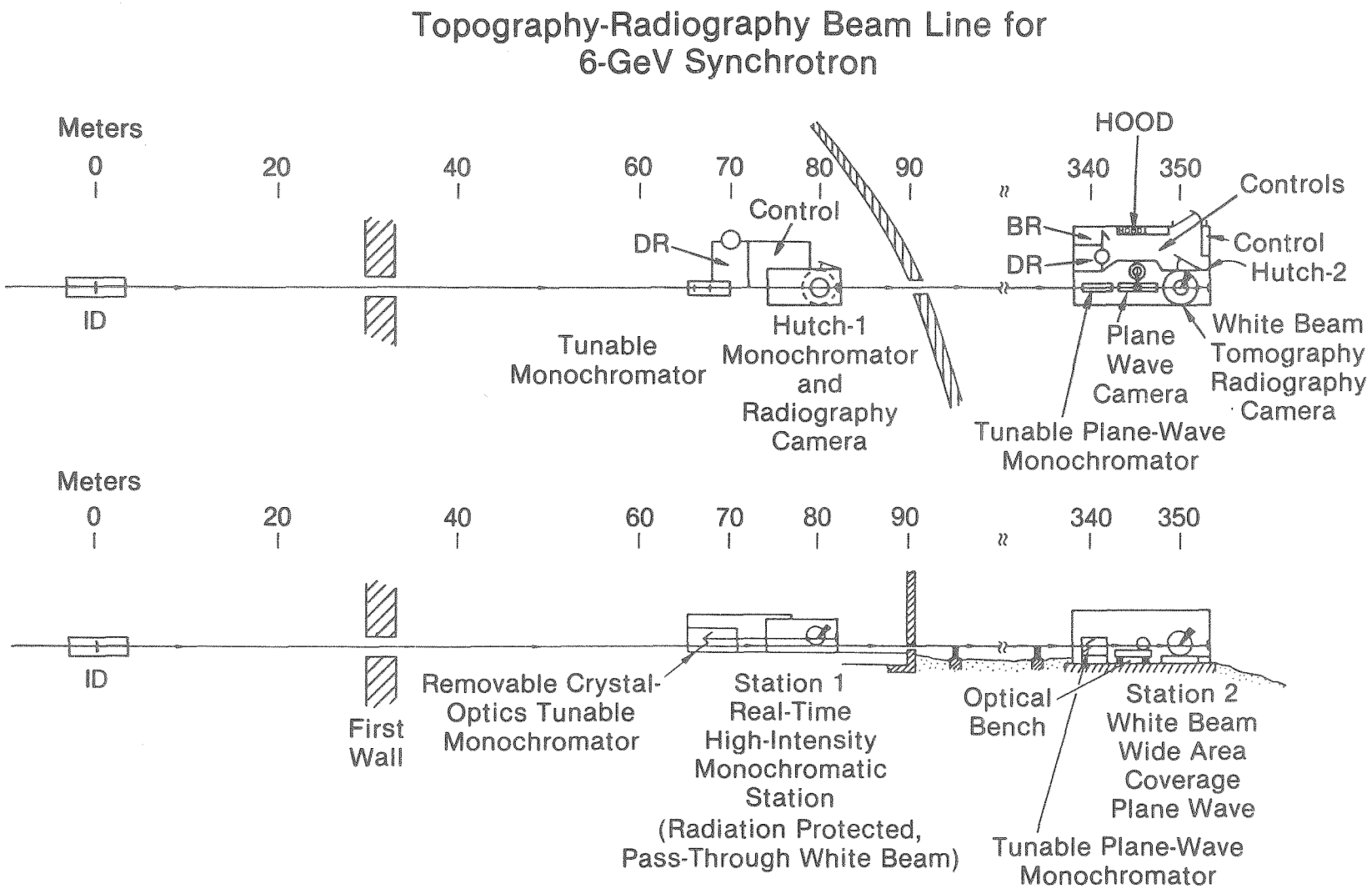

Fig. 2-1 Schematic of beamline for topography and radiography tomography

intensities, without the use of complicated and expensive optical components in the beamline. Such additional optical components can cause aberrations in images that would make topography virtually uninterpretable. In addition to the white-beam and monochromatic plane-wave cameras, Station 2 will contain control areas, hood, darkroom, and small bathroom, in a total area of ~1500 ft^2. The camera designs used for cost estimates are based on reasonable extensions of the state of the art.(2)

Resolution calculations depend on the sample-to-detector distance, the source-to-sample distance, and the source size. Area coverage depends on the vertical and horizontal divergence characteristics of the source. With a wiggler, the vertical divergence is ~0.2 $mrad^2$. The intensity available at a particular sample position can be calculated(3) and normalized to the intensity value, I_o, needed to expose a moderate-speed x-ray film. This normalization procedure follows that used by Graeff et al.(4) Thus, I/I_o gives the relative intensity available at the sample position to expose an x-ray film plate which would need a nominal 20 sec for a saturation value of $I_o \simeq 5 \times 10^7$ photons/sec/mm^2. A value of $I/I_o > 1$ means exposure times shorter than those available on current synchrotron sources. Geometric resolution, beam area coverage, and relative intensity have been calculated for Stations 1 and 2 by assuming that the performance values of the ID are identical with those of WIG2 (see Table 2-1).(3) The results are presented in Table 2-2.

Table 2.1

Parameters of Transverse Wiggler Source

E_R (GeV)	6.0
I (mA)	100
ρ (m)	16.7
B_o (T)	1.2
σ_x (mm)	0.1
σ_y (mm)	0.03
E_c (keV)	28.7
Number of Poles	20
Period (cm)	20
K	22
L (m)	2.0
Total Power (kW)	6.5
Peak Power ($kW/mrad^2$)	16.7

Table 2.2

Expected Geometric Resolution, Sample Area Coverage, and Relative Intensity at Beamline Stations 1 and 2

Station	Distance from ID (m)	Relative Intensity,[b] I/I_o Vertical	Horizontal	Geometric Resolution[a] (μm) Vertical	Horizontal	Area Coverage (mm) at 10 keV	at 50 keV
1	80	0.037	0.120	16	24	7000	3890
2	350	0.009	0.030	70	106	360	200

[a]Sample-to-detector distance = 10 cm.

[b]Based on ID parameters given in Table 2.1.

REFERENCES

1. J. C. Bilello and Z. Ref, "Synchrotron X-Ray Topography Beamline on a 6 GeV Source" to be published in Proc. Workshop on the Scientific Case for a 6 GeV Synchrotron Source, Argonne National Laboratory, Argonne, IL, December 9-11, 1985.

2. J. C. Bilello et al., to be published in Nucl. Instrum. Meth.

3. G. K. Shenoy and P. J. Viccaro, "An Overview of the Characteristics of the 6 GeV Synchrotron Radiation: A Preliminary Guide for Users," ANL Report ANL-85-69 (October 1985).

4. W. Graeff, M. Sauvage, and T. Tuomi, "Topography at the ESRF," Report No. ESRP-IRI-7/83 Rev. (1983).

3 Inelastic Scattering with Ultrahigh Energy Resolution

3.1 Introduction

Ultrahigh-resolution inelastic scattering of x-rays from condensed matter has not been used to its full potential because of the limited flux available from laboratory-based x-ray sources and their poor collimation and tunability.[1] Inelastic scattering enables the study of phonon excitations in solids. This is an area so far dominated by neutron scattering. However, x-ray scattering offers several advantages:

(1) Since x-rays couple to charge densities, one can study electronic excitations that are not accessible by neutrons.[2]

(2) Excitations that will require high energy transfers, i.e., above 200 meV, will be the unique domain of x-ray scattering.

(3) In the energy range of 50-200 meV, x-ray scattering will be complementary to neutron scattering, with the added advantage of constant momentum transfer during an energy scan. Thermal neutrons have energies comparable to excitations in solids. Therefore, during inelastic collisions, k changes considerably. This will cause multiphonon processes, which can be avoided in x-ray scattering.

A higher scattering cross section of x-rays (about 10 times higher) may be disadvantageous because of limited penetration in the bulk. However, with this technique, dynamics of surfaces can be studied. Also, the study of lattice dynamics of light impurities, collective excitations in liquids, and molecular spectroscopy of liquids will be possible.[3] With a resolution of 0.2 $Å^{-1}$ in momentum transfer, it is possible to measure dispersion curves, since Brillouin zone boundaries are 0.5 to 1.0 $Å^{-1}$.

3.2 Insertion Device

In order to study excitation in the meV range with photons of keV energies, one needs an energy resolution of $\Delta E/E = 10^{-7}$. This will require high energy rays (E > 15 keV). The experimental setup will allow the use of a highly collimated beam. Combined with the need for high fluxes, an undulator with an energy of 20 keV in the first harmonics will be required. The device parameters are given in Table 3-1.

Table 3-1

Parameters of 20 keV Undulator

Period (cm)	1.6
Gap (cm)	1.0
Length (m)	5
K	0.3
1st-Harmonic Energy (keV)	20
Total Power (kW)	0.72
Peak Power ($kW/mrad^2$)	57.8
Surface Power Density at 40m (kW/cm^2)	3.6

The details of this undulator, its design, and the associated vacuum chamber have been presented in elsewhere.(3)

3.3 Optical Elements

3.3.1 Premonochromator

This is a nondispersive, double-crystal monochromator. To pick up 20 keV, the Si (111) crystals will be at 5.7° to the primary beam. At a 40 m distance from the undulator (Fig. 3-1), the spot size on the first crystal will be ~6.7 x 69 mm. This will yield a peak power of 360 watts/cm^2, which will require cooling of the first crystal. The power density can, however, be reduced by use of filters and pinhole.

3.3.2 Spherically Bent Monochromator and Analyzer

Energy resolution in the meV range can be achieved by using higher order reflections from a Si crystal in a nearly back-scattering geometry. For silicon crystals, a $\Delta E/E$ of 10^{-7} can be achieved with (888) and/or higher order reflections. This will require x-ray photon energies higher than 14 keV. To collect sufficient intensity, a spherically bent "faceted" crystal will be used.(4) This will be a Si crystal, with 1 mm x 1 mm squares separated by 0.2-mm-deep grooves so that no elastic strains will be introduced during bending. This monochromator will be held at a fixed distance of about 55 m from the source (Fig. 3-1), and will have the necessary imaging properties. The scattering chamber which holds the sample will be directly connected to the monochromator with a beam pipe, and will be at the focal point, slightly above the primary beam (15-50 cm). There will be an option to use a focusing mirror between the premonochromator and the monochromator. An area of approximately 1 cm^2 of the incident beam will illuminate one "facet" of the bent crystal.

The analyzer will be exactly the same as the monochromator, and will be placed on a pivoted arm to scan a large range of scattering angles. The

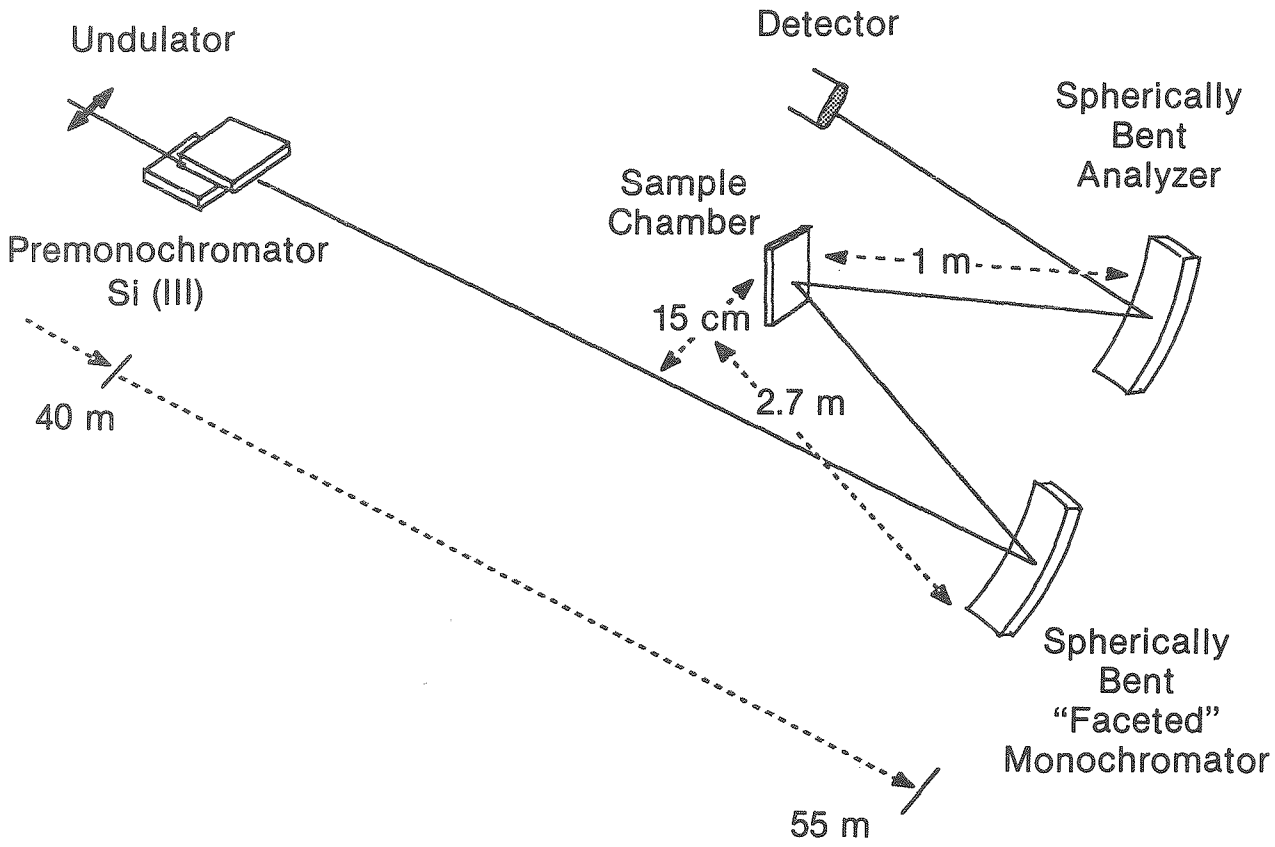

Fig. 3-1 Schematic drawing of the optical elements for inelastic scattering with ultrahigh-energy-resolution beamline

energy is scanned by varying the temperature of the analyzer crystal through changes in the lattice parameter. The analyzer temperature will be changed relative to the monochromator with an accuracy of better than 0.05°C to achieve the required energy resolution. The data will be collected as intensity versus temperature. The necessary precautions will be taken to minimize temperature gradients across the analyzer crystal.

3.3.3 Scattering Chamber

The scattering chamber with Be windows will be centered at the image point of the source. The design should be such that it will enable one to scan the energy at many scattering angles. The radiation transport is formed with evacuated beam pipes.

3.3.4 Detector

A detector with excellent efficiency for 10-20 keV photons and a sensitive area of 2 mm x 2 mm will be sufficient.

3.4 Electronics, Hardware, and Computer

CAMAC-compatible driver boards and interfaces for stepping motors will be necessary, as well as data readout interfaces. A MicroVAX II computer with a graphics terminal, printer/plotter, and Winchester disk will be used to control the spectrometer, store and reduce data, and communicate with a larger mainframe computer.

REFERENCES

1. P. Eisenberger, Synchrotron Radiation, H. Winick and S. Doniach, eds., Plenum Press (1980).
2. D. Moncton, in "New Rings Workshop," SSRL Report 83-02 (1983).
3. G. K. Shenoy, S. Kim, J. Moenich and P. J. Viccaro, "Characteristics of the Insertion Devices for the 6 GeV Synchrotron Source," Argonne Light Source Document, LS-52 (1986)
4. B. Dorner and H. Peisl, Nucl. Instrum. Meth., 208 587 (1983).

4 Surface and Bulk Studies Using High Momentum Resolution

4.1. Introduction

The elastic scattering of x-rays by matter involves momentum transfer between the radiation field and the scatterer at a constant photon energy. The resolution with which the initial and final momentum states of the photons are measured determines the precision with which the electric channels can be investigated. There are two areas described below in which a precise determination of the momentum transfer is essential in order to characterize the phenomena.

One group of experiments involves bulk studies of incommensurate structures, bond oriented and hexatic structures, substitutional compounds, phonon and polaron effects, finite-domain effects, and finite long-range correlation lengths. Each system presents a type of deviation from strict 3-dimensional structural periodicity. Consequently, a detailed 3-dimensional mapping of the scattering profile provides information which is essential for the physical characterization of these phenomena.

The structural study of these effects requires that the momentum transfer $\bar{K} - \bar{K}_o = \bar{q}$ be defined to within a value of $|\Delta\bar{q}| = \frac{2\pi}{\ell}$, where ℓ is a characteristic length of the investigated phenomenon (for example, the size of a grain boundary or the expected correlation length). In order to achieve the required resolution of $\bar{q}$, the incident-beam momentum $\bar{K}_o$ must be defined in its absolute length (i.e., energy) and also in its divergence--three variables altogether. The reflected-beam momentum $\bar{K}$ must be collected in a precise enough solid angle (two variables) to allow for the required resolution of $\bar{q}$. The stringent requirement of high resolution in 5 independent variables requires a very brilliant source, the lack of which has impeded research in this area.

Another group of experiments is related to the properties of introduction of a boundary to an otherwise infinite bulk. This boundary can be considered as another variant of the broken three-dimensional periodicity in which the characteristic direction is normal to the surface. The relevant topics in this area involve surface self-reconstruction, corrugation, surface segregation, the onset of two-dimensional melting and the associated wetting-dewetting transition, interface concentration profiles, and in-plane structures. The effectiveness of x-ray scattering in the study of surfaces is related to the phenomenon of Near Total External Reflection at grazing incidence. This effect is the basis for a number of surface-sensitive x-ray methods such as glancing angle diffraction, Near Total External Fluorescence, Reflection Extended X-Ray Fine Structure, and Fluorescence Extended X-Ray Fine Structure. In the case of liquid surfaces, it is highly desirable that the polarization vector of the x-ray beam be vertical so that the diffraction plane will be close to horizontal. We propose here a preliminary version of a beamline capable of high momentum resolution with $|\Delta\bar{q}| \leq 5 \times 10^{-4}$ Å^{-1}, suited for a high-brilliance source such as the 6 GeV Light Source.

4.2 Insertion Device

A preliminary choice of ID is a multipole wiggler with a critical energy of $E_c = 9.6$ keV. The magnetic field lines are horizontal, resulting in vertical on-axis polarization. The advantage of a wiggler over an undulator is that it provides a white source and hence permits tunability of incident x-ray energy with monochromators. This feature is important if fluorescence experiments are planned. However, the brilliance of a comparable undulator at the first-harmonic peak is greater, by an order of magnitude, than that for the wiggler. Unfortunately, the appropriate undulator would have a gap of

about 3 cm, which is much smaller than the horizontal beamline aperture necessary for the 6-GeV ring. Hence it is hard to design such an undulator. Table 4-1 describes the properties of the wiggler we have chosen. The energy range initially needed is approximately 4-15 keV.

Table 4-1

Parameters of the 9.6 keV Wiggler

Critical Energy (keV)	9.6
Period (cm)	25
Number of Poles	40
Length (m)	5
K	9.3
Vertical Opening Angle, θ_v (mrad)	1.7
Horizontal Opening Angle (mrad)	0.17
I (mA)	100
Total Power (kW)	1.8
Peak Power (kW/mrad^2)	11.2
Peak Power Normal at 25 m (kW/cm^2)	1.8
Flux at E_c (ph/sec/0.1%BW/mrad θ_v)	3.8×10^{14}

4.3 Optical Elements

In order to achieve high resolution of $\bar{q}$, one must define both the incoming momentum $\bar{K}_o$ in its 3 perpendicular directions and the scattered momentum $\bar{K}$ within a given solid angle. The divergence of the incoming beam will be controlled by a pair of vertical and horizontal entrance and exit slits upstream from the monochromator at 32 m from the sample. The longitudinal resolution will be achieved by a conventional double-crystal monochromator with crystal normal in the horizontal direction (see Fig. 4-1). Energy resolution will be traded off to gain flux, and optimized by using appropriate crystals. At 4 keV, assuming a worst case of a Si(111) crystal at 32 m as the first element, the peak power on the crystal surface will be approximately 540 W/cm^2. The slits will reduce the total power to less than 60 W in an area of 3 mm × 5 mm. The scattered radiation will be collected with a set consisting of an analyzer crystal and a linear detector oriented perpendicular to each other.

The design parameters specify high solid-angle resolution ΔK_x and ΔK_y and similar resolution in the longitudinal direction ΔK_z, with each less than 5×10^{-4} $Å^{-1}$. The designed energy range for the incident beam is from 4 keV to about 15 keV; the energy is not tunable in real experiment time. The beam size at the sample is chosen to be about 1 mm x 1 mm at 35 m from the source. This requires the divergence to be smaller than 70 μrad at 15 keV for both the incident beam and the scattered beam.

The source size for the wiggler in the horizontal and vertical dimensions does not exceed 0.5 mm. The beamline free path ℓ that is required to obtain a source size of 1 mm x 1 mm with a divergence of 70 μrad is 35 m, as calculated from the equation $\Delta K_i^o = K_o (\zeta_i + S_i)/\ell$, where ζ_i and S_i are the

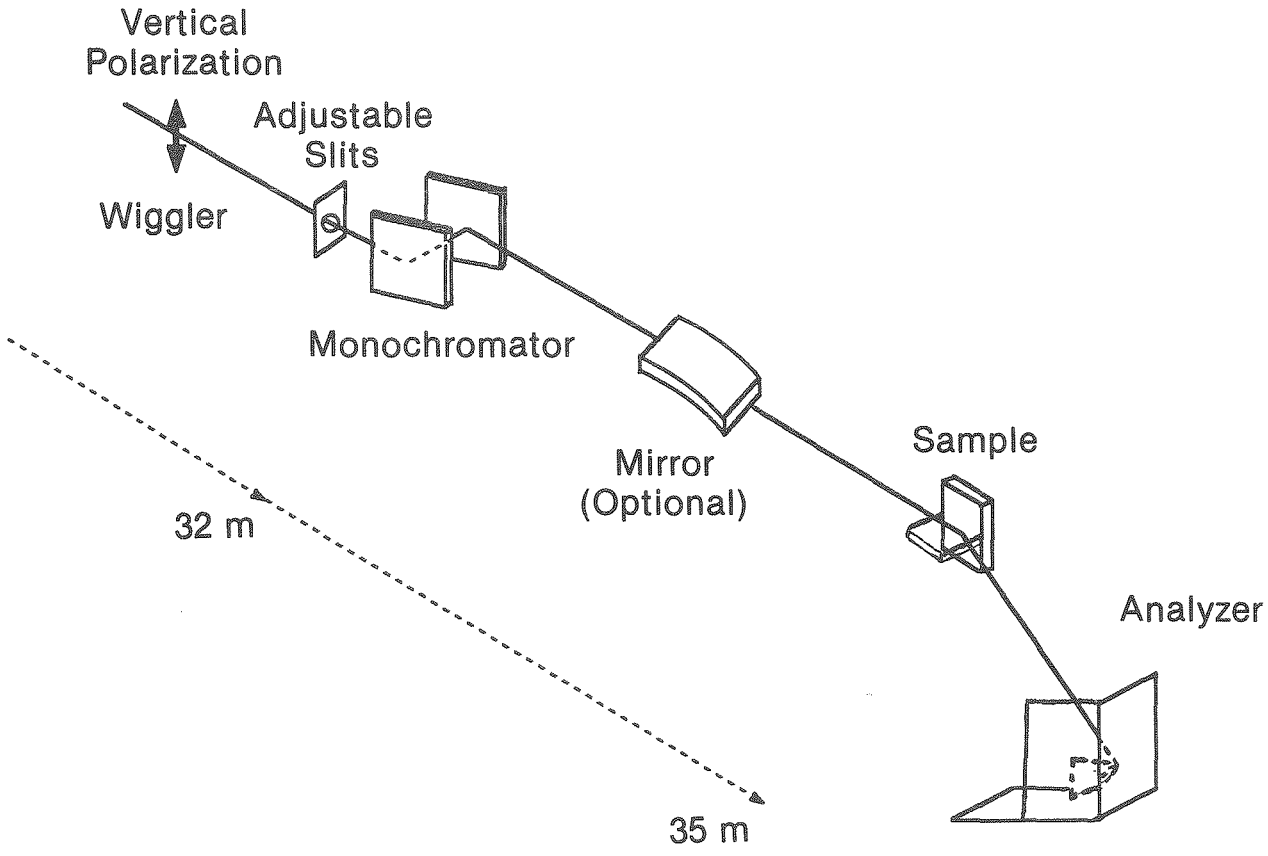

Fig. 4-1 Schematic drawing of the high-momentum-resolution beamline. Two types of samples are shown.

source size and the spot size in the i direction (i = x,y). The longitudinal divergence is given by

$$\Delta K_z^o = \Delta K_y^o \sin \theta_{Bragg} + K_o \cot\theta \cdot \Delta\theta_{Darwin} \qquad (4\text{-}1)$$

where θ_{Bragg} is the Bragg angle crystal and $\Delta\theta_{Darwin}$ is the Darwin width of the monochromator crystal. The intensity throughput of the monochromator is determined by $\Delta\theta_{Darwin}$. The optimized monochromator crystal is chosen so that the first and second terms in Eq. (4-1) are of the same order of magnitude.

Following the last criterion, the best matched crystal should have $\Delta\theta_{Darwin}$ width of the order of 0.2 mrad. A crystal with smaller $\Delta\theta_{Darwin}$, such as the Si(111) with $\Delta\theta_{Darwin}$ = 0.02 mrad, will not benefit the momentum resolution but will pass only 10% of the usable beam. Our choice will probably be a pair of asymetrically cut Ge crystals in the non-dispersive mode. Such crystals can be chosen to pass 50% of the usable radiation. For higher bandpass, multilayer elements will be tested (see Section 3.8).

The monochromator will be located at 3 m from the hutch and 35 m from the source point (see Fig. 4-1). For the diffraction experiments, we will use a regular 4-circle diffractometer equipped with microstepping control. The 2θ arm of the diffractometer will be 2 m long and support a single Ge(111) crystal in the vertical plane direction followed by a linear detector in the horizontal direction with positional resolution of 50 μm. For diffraction from surfaces of liquids, a custom-made diffractometer will be used. A flat mirror will tilt the beam downwards at the desired glancing angle. A trough and a 2θ arm will be set on a coaxial circle. The trough will also be able to move in the vertical direction with an accuracy of 2 μm. The detector setup will again be a combination of a Ge(111) crystal and

a linear detector, perpendicular to each other and moving in the horizontal plane with a 2-m arm.

4.4 Electronic Hardware and Computer

Several data readout boards and interfaces for the detectors will be needed, as well as driver and control boards for the stepping motors. All are CAMAC compatible. These will be controlled by a microVAX II computer which will also provide for communication with the mainframe and initial data reduction. The computer station should contain a graphics terminal with a printer/plotter and Winchester disk.

5 Inelastic Scattering from Charge and Spin

5.1 Introduction

The inelastic scattering of x-rays provides valuable information concerning various aspects of electrons in solids. The beamlines described here will allow inelastic scattering experiments at two different energy ranges.

The first energy range is that of Compton scattering, which involves incident energies above 20 keV for most systems. At these energies, the scattered-energy distribution versus angle (Compton profile) is related to the momentum distribution of the electrons in the solid. Precisely measured Compton profiles reflect anisotropies in electronic distributions and, when circularly polarized x-rays are used, the momentum profiles of the magnetic electrons can be extracted (magnetic inelastic scattering). The relative energy resolution $\Delta E/E$ necessary for this class of experiments is approximately 10^{-4}, and detection at large scattering angles is required.

The second energy range involves low incident x-ray energies of approximately 3 to 5 keV. The inelastic component of the scattering involves transitions between electronic states near the Fermi energy and contains information concerning the dynamic structure factor $S(E,q)$ where E and q are the energy and momentum transfer, respectively. Energy resolutions between 100 meV and 1 eV are needed, resulting in a relative energy resolution of $\sim 10^{-4}$. The detection angle of the scattered x-ray is variable so as to permit variation of q and the inelastic part of the scattered radiation is determined by energy analysis.

Although the two processes involve different energy ranges, many of the optical elements defining the incident beam are equivalent. A single

straight section could be used with a carousel arrangement of the two wigglers.

5.2 Compton and Magnetic Inelastic Scattering

5.2.1 Insertion Device

The device selected is a multipole wiggler with a critical energy of 28 keV. This guarantees sufficient flux at up to 60 keV. The parameters of this wiggler (WIG2) are given in Table 2.1.

5.2.2 Optical Elements and Detector

Premonochromator. A premonochromator consists of a non-dispersive pair of cooled Si(111) crystals at a distance of 32 m from the source point (see Fig. 5-1). At this distance, the normal peak/power is $P_A \simeq 3300$ W/cm^2. For energies near 50 keV, the angle of incidence on the Si crystal is approximately 2.3° and the peak power on the first crystal is approximately 130 W/cm^2. Absorbers and filters that absorb the lower energy can be used to remove part of the spectrum, which will reduce the power considerably. The crystal sizes necessary are less than 10 cm by 25 cm. Cooled slits will be used to define the beam if necessary.

Vertical Focusing Mirror. A singly curved, vertical-focusing, Pt-coated elliptical mirror at 36 m has its focal point at the sample at approximately 8 m downstream (see Fig. 5-1). In order to reflect 50-keV radiation at 36 m, a mirror length of 3 m is necessary. The preliminary plan is to dynamically bend a flat mirror to the required radius. Without the mirror, the beam size in the vertical direction at the sample would be approximately 0.9 cm.

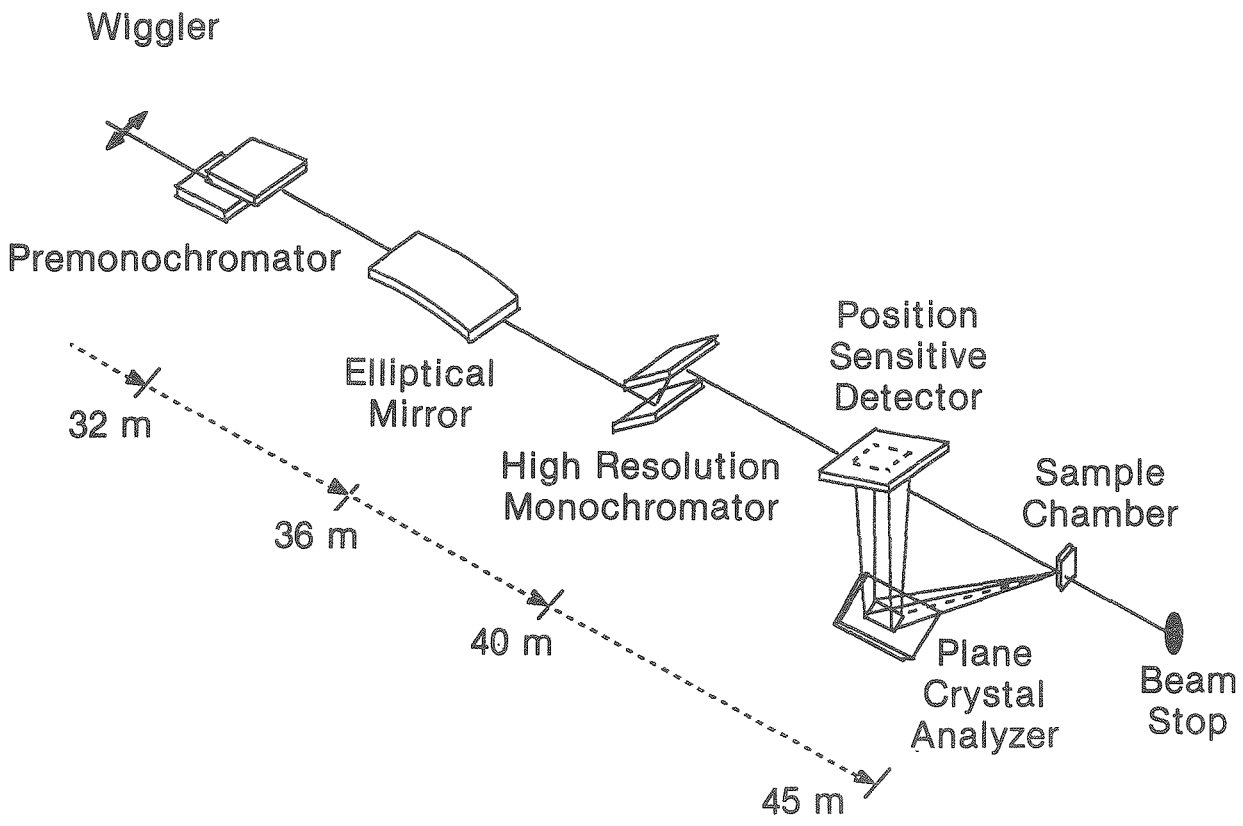

Fig. 5-1 Schematic drawing of the Compton/magnetic inelastic scattering beamline

High-Resolution Monochromator With Sagittal Focusing. In order to provide the necessary resolution of $\Delta E/E \sim 10^{-4}$, a second monochromator at a distance of 40 m from the source point is used. It consists of two Si(220) crystals in which the second crystal is cylindrically bent to provide sagittal focusing. For magnetic inelastic scattering where circularly polarized x-rays are necessary, a polarizing monochromator described by Golovchenko[1] is proposed. The physical arrangement is similar to that of the dispersive monochromator. However, the second reflection uses a Laue geometry in which the polarization vector of the incident beam is at 45° to the plane. The transmitting crystal acts as a quarter-wave plate for a given crystal thickness and can produce left- or right-hand circularly polarized x-rays. The monochromator chamber is vacuum compatible.

Sample Chamber. A controlled-environment, vacuum-compatible (10^{-4} Torr) sample chamber contains a sample holder at the focal point of the incident beam at approximately 45 m from the source point. The scattered beam should be scanned over at least one quadrant. All the necessary positioning devices and temperature measurements and control probes are enclosed. Beam pipes extend from the monochromator to the sample chamber and from the chamber to the analyzer.

Crystal Analyzer. Energy analysis at a given scattering angle is achieved by a plane crystal Si or Ge monochromator at approximately 1 m from the sample. This element is energy dispersive and is used in conjunction with a position-sensitive detector. The combined resolution is a function of the rocking curve of the crystal and spatial resolution of the detector, and should be at least 10^{-4}.

Monitor Detector. It is advisable to include a second detector on the same radial scattering circle in order to monitor Bragg reflections and

harmonic content and background of the scattered beam.

Electronic Hardware and Computer. A MicroVAX II computer with a graphics terminal, printer/plotter, and Winchester disk drives is necessary. Data will be received from readout interface boards from the detectors. Drivers for stepping motors and associated hardware are included. The computer can also be used to perform preliminary data reduction and analysis and to transmit data to a mainframe computer. The electronic hardware should be CAMAC compatible.

5.3 Intermediate-Resolution Low-Energy Inelastic Scattering

5.3.1 Insertion Device

The device selected is a multipole wiggler with a critical energy (E_c) of 2.4 keV. The relevant parameters are given in Table 5-1.

5.3.2 Optical Elements and Detector

Premonochromator. The premonochromator described in Section 5.2.2 will be used. At an energy of 3 keV, the Bragg angle for Si(111) is approximately 41°. At this angle and 32 m from the source, the peak power on the first crystal is approximately 50 W/cm^2.

Vertical Focusing Mirror. The vertical focusing mirror described in Section 5.2.2 will be used. The critical angle for Pt at 50 keV is also appropriate at 3 keV, but a larger grazing angle may be chosen.

High-Resolution Monochromator with Sagittal Focusing. A dispersive high-resolution monochromator at 40 m with sagittal focusing similar to that described in Section 5.2.2 can be used. The focusing properties of the mirror and second crystal in this arrangement are identical with that for the Compton-scattering beamline.

Table 5-1

Parameters of the 2.4 keV Wiggler

E_c (keV)	2.4
Period (cm)	83
Number of Poles	12
Length (m)	4.98
K	7.8
B_o (T)	0.1
Vertical Opening Angle (mrad)	0.17
Horizontal Opening Angle (mrad)	1.3
Current (mA)	100
Total Power (W)	60
Peak Power ($W/mrad^2$)	836
Flux at E_c (ph/sec/01%BW/mrad θ)	$6x10^{13}$

Sample Chamber. A controlled-environment, vacuum-compatible chamber contains the sample at the focal point of the mirror and last monochromator crystal (Fig. 5-2). The chamber houses the necessary temperature probes, control devices and sample positioning micrometers. The scattered radiation is collected in the vertical plane by using a spherically bent focusing crystal of Si or Ge. The diffraction planes can be the same as the monochromator and the scattered radiation is focused at 1 m into an integrating detector. Other scattered beam monitors may be necessary. The angular variation should be over one quadrant in the vertical direction, with the beam tube carrying radiation to the sample and to the various detectors.

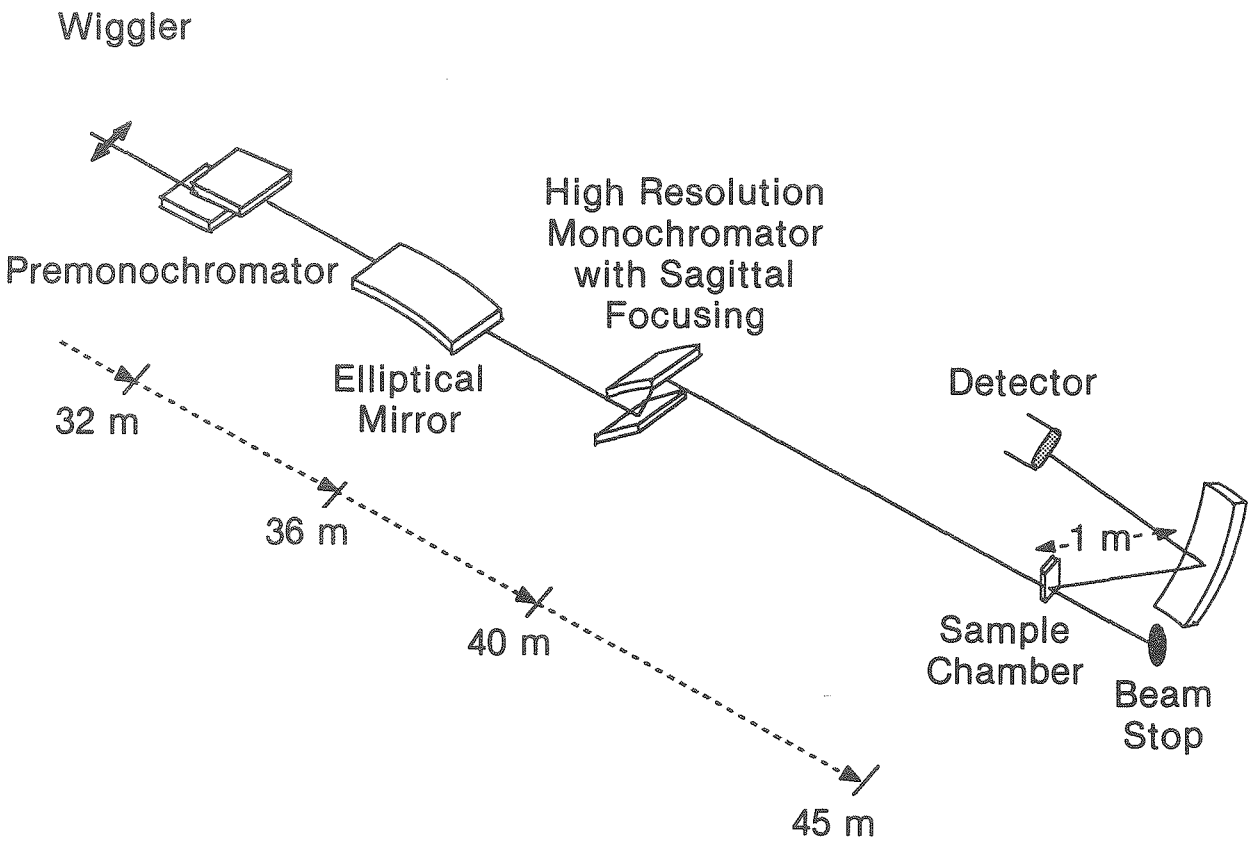

Fig. 5-2 Schematic drawing of the low-energy inelastic scattering beamline

REFERENCE

1. Golovchenko, J. A., in SSRL Report 83/102, ed. K. Cantwell and C. Mitchell, (1983), p. 147.

6 Advanced X-Ray Photoelectron Spectroscopy Studies

6.1 Introduction

The soft x-ray region of interest spans the energy range from 100 to 1500 eV. This includes the domain of conventional x-ray photoelectron spectroscopy (XPS) and extends down in energy. In recognition of the ability of the 6 GeV machine to generate useful low-energy radiation, the Soft X-Ray Working Group at the 6 GeV Scientific Workshop (held at Argonne in December 1985) endorsed the recommendation that one soft x-ray beamline be developed for advanced XPS applications. These include high-energy, spatial, and/or spin resolution studies. High-energy resolution is valuable because the shallow, and hence sharp, core levels are found in this energy range. It is desirable to monochromate the beam at least to match the intrinsic lifetimes of the core holes ($\sim$ 0.2-1 eV) in order to accurately measure chemical shifts. It should be possible, with grating monochromators, to obtain resolutions approaching 0.1 eV at 1 keV. Small spot size ($<<$ 1 mm) is a natural consequence of the high brilliance of the undulator radiation, coupled with the image reduction capability of the monochromator. The high flux and brilliance will also be utilized in spin-resolved XPS experiments to study novel magnetic materials of basic and technological interest. The tunability of the photon energy translates into a variable photoelectron mean free path for nondestructive depth-profiling studies, as well. A separate class of high-momentum-resolution scattering experiments that require high brilliance but not high energy resolution will also be possible on this beamline in the soft x-ray region. These experiments are discussed with respect to higher energy x-rays in Section 4.

It is proposed that a new adaptation of the plane-grating monochromator (PGM) concept be incorporated into the soft x-ray beamline. The plan is to fully utilize the spatially structured nature of the undulator beam profile. The brightness and brilliance of the source will be exploited by accepting only a part of the undulator beam, via a variable aperture. This will permit photon energy scanning at high throughput without undulator gap adjustments. The small spot size achievable will permit the use of small and, hence, more perfectly figured optical elements than those presently in use. It is the quality of such elements that, thus far, has been the limiting factor in resolution at existing sources.

6.2 Undulator Characteristics

The undulator will be an adjustable-gap device, primarily intended for operation with first-harmonic radiation. Table 6-1 lists the parameters of the proposed undulator. By tuning the gap, one can vary the K values between 1.5 and 5; the (on-axis) first harmonic can thus be tuned between roughly 250 and 1600 eV. The design concept proposed here merges the undulator source with a PGM that utilizes off-axis first-harmonic radiation to obtain a high flux of (brilliant) radiation over a wide and continuous spectral range.

An undulator beam is a highly directed polychromatic source with a spectral distribution of photons with energies that decrease with radial distance from the beam center. The radiation in specified monochromatic windows appears in concentric circles of the beam cross section (as shown in Fig. 6-1a). On moving off-axis from the central beam in any direction, the photon energy spectrum shifts to lower energies. Off-axis motion in the vertical direction allows for spectral tunability without excessive loss of

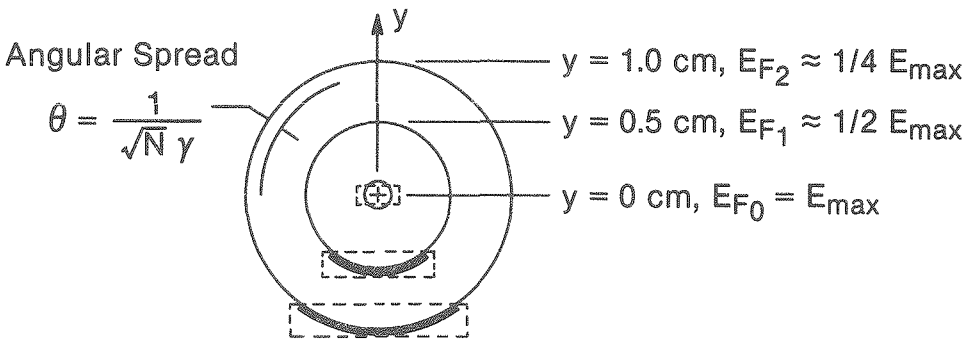

Photon Beam Cross-Section for R ≈ 25-30 m

(a)

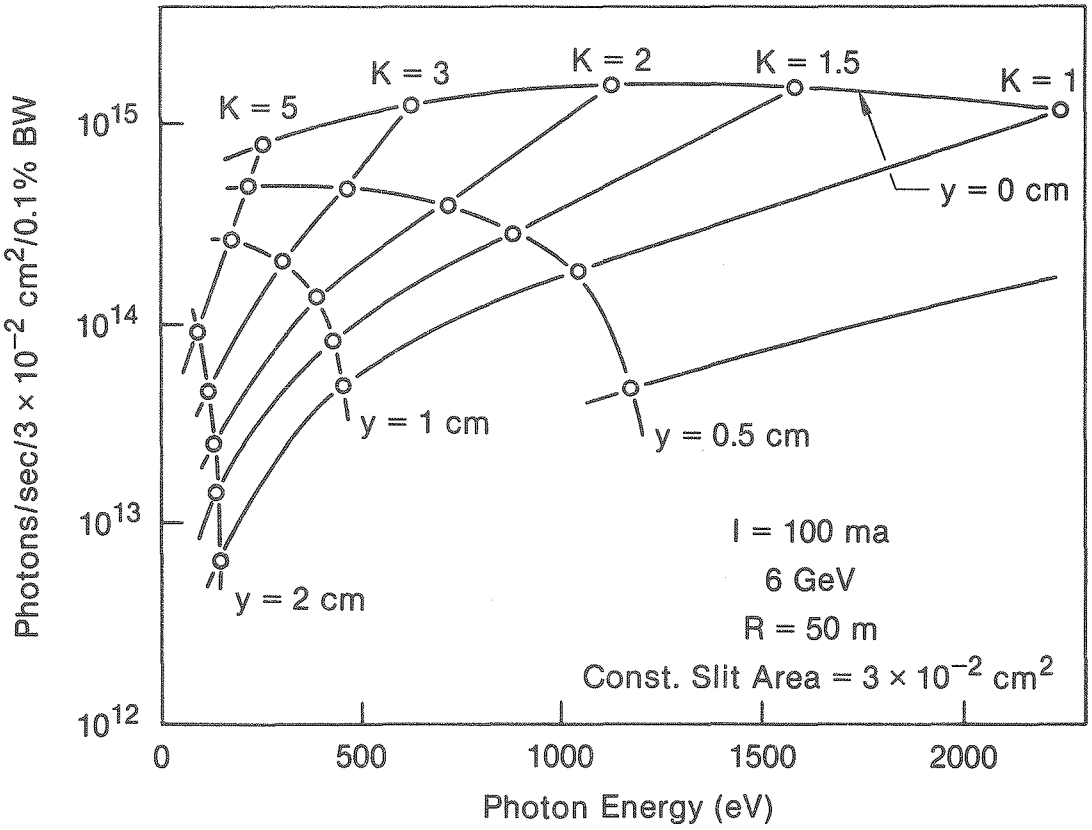

(b)

Fig. 6-1 a) Undulator source cross section at 25-30 m and (dashed lines) rectangular variable aperturing of the beam
b) Brightness vs photon energy for different K values and aperture setting

Table 6-1

Parameters for Undulator[a] with Adjustable Magnet Gap

	Minimum Gap	Maximum Gap
Gap (cm)	3.6	7.0
B_o (T)	0.54	0.16
K	5.04	1.50
On-Axis 1st-Harmonic Energy (eV)	249	1607
Total Power (kW)	3.3	0.29

[a]Calculated for a 5-m-long undulator with 50 periods, each 10 cm in length.

intensity. Fig. 6-1b shows the flux in a 0.1% bandpass through a horizontal slit of constant size that is moved along the vertical to accept radiation at different off-axis distances (y). The figure shows lines of constant K intersecting lines of constant y.

Because monochromatic radiation appears in a ring, it is advantageous to have an entrance slit whose length increases with y, thus permitting utilization of a maximum amount of the monochromatic circle consistent with the effective slit width (which is determined by the grating illumination). Minimizing slit length and slit width consistent with optimal passage of the bandpass of interest means that the dominant heat-absorbing element will be the entrance slit, a cooled variable aperture. The variable aperture thus serves as (1) a premonochromator, by utilizing the natural dispersion of the undulator beam, (2) the dominant heat- absorbing element, and (3) a beam-size reduction device for optimizing brilliance.

6.3 The Aperture and Filter Mirror

A schematic of the variable aperture is shown in Fig. 6-2a. The aperture is computer controllable in synchrony with the monochromator spectral tuning. The maximum radiated power at K = 5 is 3.3 kW, though greater heat loadings would be encountered if higher K operation were considered. General operation will be at K = 1.5, where the total power is only 290 W.

Fig. 6-2b shows schematically the aperture, mirror, and monochromator. The mirror (M_0) is a cooled Si single crystal placed at grazing incidence to the photon beam. It can be translated a distance of 1 m on an air bearing to scan across the photon beam (in the vertical direction) and to reflect the desired bandpass of radiation down the monochromator axis. Single-crystal silicon is used for M_0 for the following reasons:

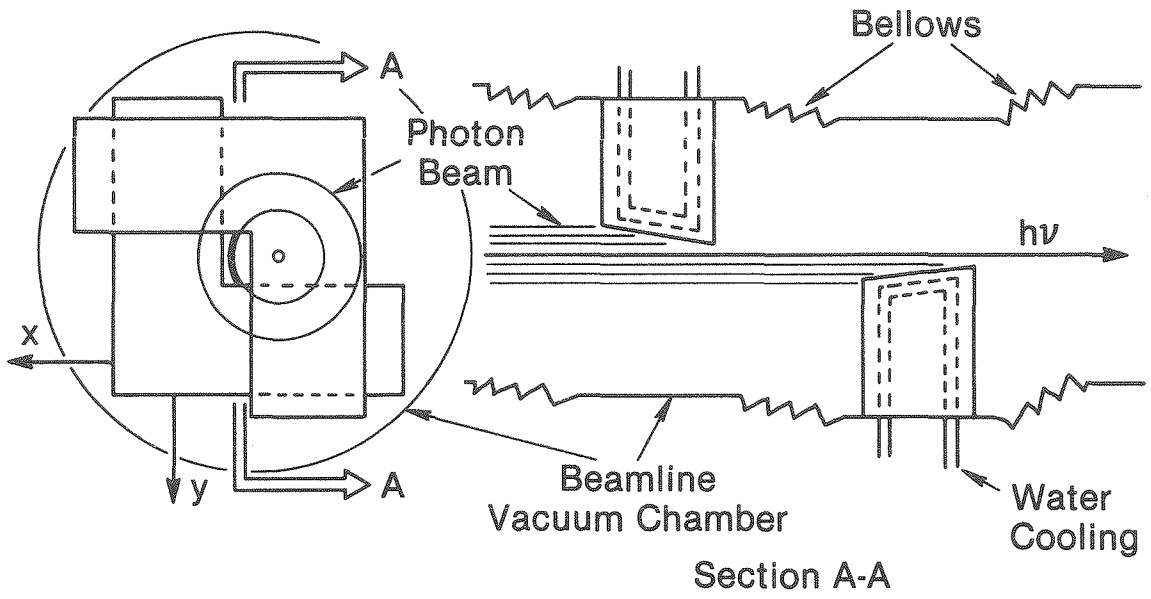

Variable Aperture

(a)

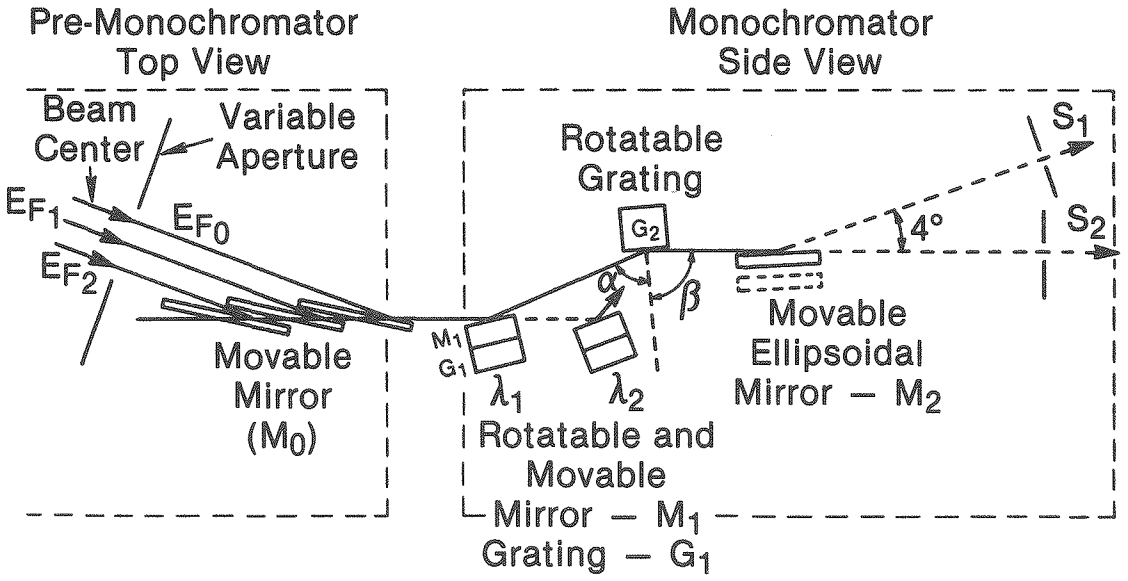

(b)

Fig. 6-2 a) Schematic of the variable aperture. (Left) front view; (right) side view b) Schematic of the premonochromator-monochromator lay-out

(1) Because of its good thermal properties, it can accommodate substantial heat loading without severe distortion or damage. (2) It can be made optically flat. (3) At a 0.7° photon incidence, it serves as a low-pass filter with a cutoff at 2500 eV. (4) Silicon fabrication technology is well developed; mirrors are readily available and reasonably inexpensive.

6.4 The Monochromator

Below a 1000 eV photon energy, one is constrained to use grating monochromators in the grazing-incidence mode. Ray tracing studies are required to optimize the match of the monochromator with the undulator source.

The recent conceptual design of an undulator monochromator (UMO) by Brown and Hulbert apparently offers the best characteristics for the present application. It consists of three optical elements (Fig. 6-2b), the first two of which are a plane movable mirror and a plane rotatable grating. The final mirror is an ellipsoidal focusing mirror (removable for momentum resolution studies).

The UMO resolution will depend on the source size. In the "virtual source" mode, the resolution will exceed the ERG resolution for gratings with equal D-spacing. It can be shown that

$$\Delta E = E^{3/2}\ \Delta\zeta/99.5\ [D(C^2 - 1)]^{1/2}\ ,$$

where D is the grating spacing and C is a constant that relates the incident and exit angles. Using a C of 2.25, as suggested by Brown & Hulbert, a grating of 1200 lines/mm, and a $\Delta\zeta$ determined from the size and angular divergences of the positron beam in the undulator, one obtains ultimate

resolutions approaching 10 meV at 100 eV, or 300 meV at 1000 eV. Use of a 2400-line/mm grating is feasible, and would further improve the resolution.

Table 6-1 contains design information for an adjustable-gap undulator. Table 6-2 shows the off-axis positions (y) corresponding to various radiation energy levels in a soft x-ray beamline. For each energy level, Table 6-2 also gives the effective slit width and length to which the variable aperture will be adjusted, and the projected heat loadings and maximum power densities expected on the various elements of the system. Projected throughputs for operation in the virtual-source mode are also listed. When the undulator is gap-tuned to the appropriate K setting, throughput flux (uncorrected for reflection losses) for the entire spectral range (250-1600 eV) exceeds 10^{14} photons/sec in a 0.1% bandpass. Reflection losses may reduce this transmission by about an order of magnitude. Of equal importance, a significant high-flux spectral range is available at all K settings with intensities that vary smoothly across that spectral range. For on-axis operation, the spectral brilliance is very high. Furthermore, a high (and smoothly varying) brilliance is available over a wide spectral range at all K settings.

Special adaptations of the PGM are incorporated for maximum momentum or energy resolution. Given that the final optical element, the refocusing mirror (M_2), of necessity destroys the momentum purity of the photons, it will be mounted on a motion device so that it can be removed from the beam path. This will necessitate the use of a separate slit, S_2 (shown in Fig. 6-2b), since the beam is no longer reflected by M_2 into the slit S_1. To achieve state-of-the-art energy resolution, a two-grating mode of operation will be used. The second grating will be mounted behind the M_1 mirror.

A conventional flipper will provide the rotation to enable the grating G_1 to replace the M_1 mirror. Since all the motions are computer controlled, it should be relatively simple to position the grating G_1 to yield a double-grating monochromator. Since this may decrease the flux by an order of magnitude or more, it is clear that such an operation requires a high-brightness source, and should be invoked only when additional resolution is essential. This additional capability is cost effective in the sense that all motion and external adjustments are already built into the system. The focusing mirror M_2 is positioned so that the exit rays are parallel to the incoming beam (see Fig. 6-2b) in both the single and double-grating modes of operation.

The three modes of operation of the soft x-ray beamline are summarized in Table 6-3.

The flexibility of the present PGM design permits further improvements. Throughput increases can be expected if appropriately blazed gratings become available. Ray tracing can determine the optimal shape of the exit slit. For low-K operation, the $SmCo_5$ permanent magnets used in the undulator could be replaced by magnets (such as Alnico) with weaker fields.

Table 6-2

Parameters Corresponding to Various Energies for Soft X-Ray Beamline Operating at K = 15[a]

E (eV)	y (cm)	Aperture Size (cm)		Flux at 0.1%BW (10^{14} ph/sec)	Brilliance at 0.1BW (10^{17} units)	Absorbed Power (W) at			Maximum Power Density (W/cm^2) at	
		Width	Length			Aperture	M_0 (>2.5 keV)	G_2 (0-2.5 keV)	M_0	G_2
1600	0.02	0.14	0.16	4	12	256	28	10	22	10
1400	0.12	0.15	0.38	2	-	237	38	18	13	8
1200	0.18	0.16	0.48	1	3	251	22	21	7	7
1000	0.24	0.18	0.58	0.9	-	266	11	17	3	5
800	0.31	0.20	0.70	0.7	1	277	11	16	2	3
600	0.40	0.23	0.86	0.5	-	285	0.2	9	0.6	2
400	0.54	0.28	1.10	0.4	0.5	290	0.1	4	0.2	0.5
200	0.82	0.39	1.61	0.2	-	293	<1	0.9	0.02	0.08

[a] $R = 25$ m $K_{rms} = 1.061$
$L = 5$ m $I = 100$ mA
$\lambda = 10$ cm $P_{total} = 290$ W
$G = 7$ cm Max. On-Axis Power Density = 1.8 kW/cm^2
A reflectivity of 1 is assumed for all reflecting elements.
M_0 cutoff = 2.5 keV = R_c
θ cutoff = 0.7°

Table 6-3

Comparison of Three Modes of Operation of Soft X-Ray Beamline

Mode	Energy Resolution	Throughput
Conventional PGM (Virtual Source or Constant Blaze)	High	High
High-Momentum Resolution	Low	High
Double Grating	Very High	Low

7 Small Angle X-Ray Scattering Studies

7.1 Introduction

Small angle scattering from substances is one of the classical methods widely used in biology, polymer science, chemistry, geology, materials science, and physics to study the variation of scattering density (or equivalent chemical composition) over distances which span $10 < d < 1000$ Å. The primary quantities of interest are the size, density or molecular weight, and shape of the scattering entities. In cases where the scattering centers span a specific size distribution, a knowledge of the distribution statistics is also important. Given the size range $10 < d < 1000$ Å, it is clear that overlap with complementary techniques (e.g., electron microscopy) is very important.

The variation of scattering density over significant distances gives rise to small angle scattering. If $\vec{k}_i$ and $\vec{k}_f$ are wavevectors for incoming and outgoing elastically scattered photons with wavelength λ ($k_i = k_f = 2\pi/\lambda$), then the scattering vector is defined by

$$\vec{Q} = \vec{k}_i - \vec{k}_f \ ,$$

and $Q = 4\pi \sin\theta/\lambda$, where 2θ is the measurable quantity. In the limit of small angle measurements,

$$Q \sim \frac{2\pi\theta}{\lambda} \ . \qquad (7\text{-}1)$$

The small angle scattered intensity I(Q) is given by

$$I(Q) \approx d\sigma/dR = \left| \int_{V_s} \rho_f(\vec{r}) \exp[i\vec{Q}\cdot\vec{r}]\, d^3r \right|^2, \qquad (7\text{-}2)$$

with integration limits set by the sample volume illuminated by the x-ray beam. The scattering density function $\rho_f(\vec{r})$ is defined by

$$\rho_f(\vec{r}) = f(\vec{r})\, n(\vec{r}), \qquad (7\text{-}3)$$

where $f(\vec{r})$ is the form factor of the scattering entity at position $\vec{r}$ and $n(\vec{r})$ is the number density of scatterers at $\vec{r}$. In the case of homogeneous scattering centers and surrounding matrix, Eq. (7-3) can be given as

$$d\sigma/dR = N_p V_p^2 (\rho_p - \rho_m)^2 S(Q)\, \psi(Q) \ . \qquad (7\text{-}4)$$

Here S(Q) is the effective particle scattering function and $\psi(Q)$ is the particle-particle interference function. Particle shape and size information is contained in S(Q). The Fourier transform of S(Q) gives us the desired real-space definition of the scattering entities.

To obtain information about large particles (d = 200-1000 Å) and to precisely define the shape of the scattering centers requires information at very small Q values. For 1000-Å spherical particles we might assume the Gunier region extends to $Q \lesssim 1.5\ R = 3 \times 10^{-3}$ Å^{-1}. For non-spherical particles, this Q value must be substantially reduced. To obtain a reasonable number of equally spaced intensity measurements at constant Q^2 intervals, one requires $Q_{min} \approx 5 \times 10^{-4}$ Å^{-1}, with resolution $\Delta Q \sim 10^{-4}$ Å^{-1}.

Small Q scattering at relatively low photon energies requires transmission of the incident beam through the sample. Since absorption cross sections for most materials are large, the transmitted beam can be easily reduced by 1/e for sample thicknesses in the μm range. To prepare samples with uniform thickness requires us to consider incident-beam dimensions $A_B < 1$ mm × 1 mm at the sample position.

7.2 Undulator

The conditions of low incident-beam divergence and high brilliance are ideal synchrotron characteristics for small angle scattering measurements. The insertion device for our very low-Q, high-resolution small angle scattering diffractomer will be an undulator with $\lambda = 3.8$ cm and $1.8 \leq G \leq 3.5$ cm (as described in Ref. 1 of Section II.9). The first-harmonic energy range will be $5 \leq E \leq 8$ keV. The undulator will have a brilliance (BR) $\sim 10^{18}$ ph/sec/0.1%BW/mrad^2/mm^2; a beam size of $\sigma_x \sim 0.4$ mm and $\sigma_y \sim 0.1$ mm; and a beam divergence of $\sigma'_x \sim \sigma'_y \sim 0.2$ mrad. For reasons which will be discussed later, we will discount higher order harmonics, although if other monochromator crystals were selected, second and third harmonics could be utilized.

7.3 Monochromator Assembly

A partial simplified schematic diagram of the proposed instrument is given in Fig. 7-1. In view of the above-mentioned requirement for small Q, we haven chosen a four-crystal assembly. The monochromator crystals C1 and C2 are asymmetrically cut Si(111) crystals. Crystals C3 and C4 are designed to provide energy resolution $\Delta E/E \sim 2 \times 10^{-4}$ and to reduce the "parasitic" scattering from the tails of the ideal crystal rocking curve. For

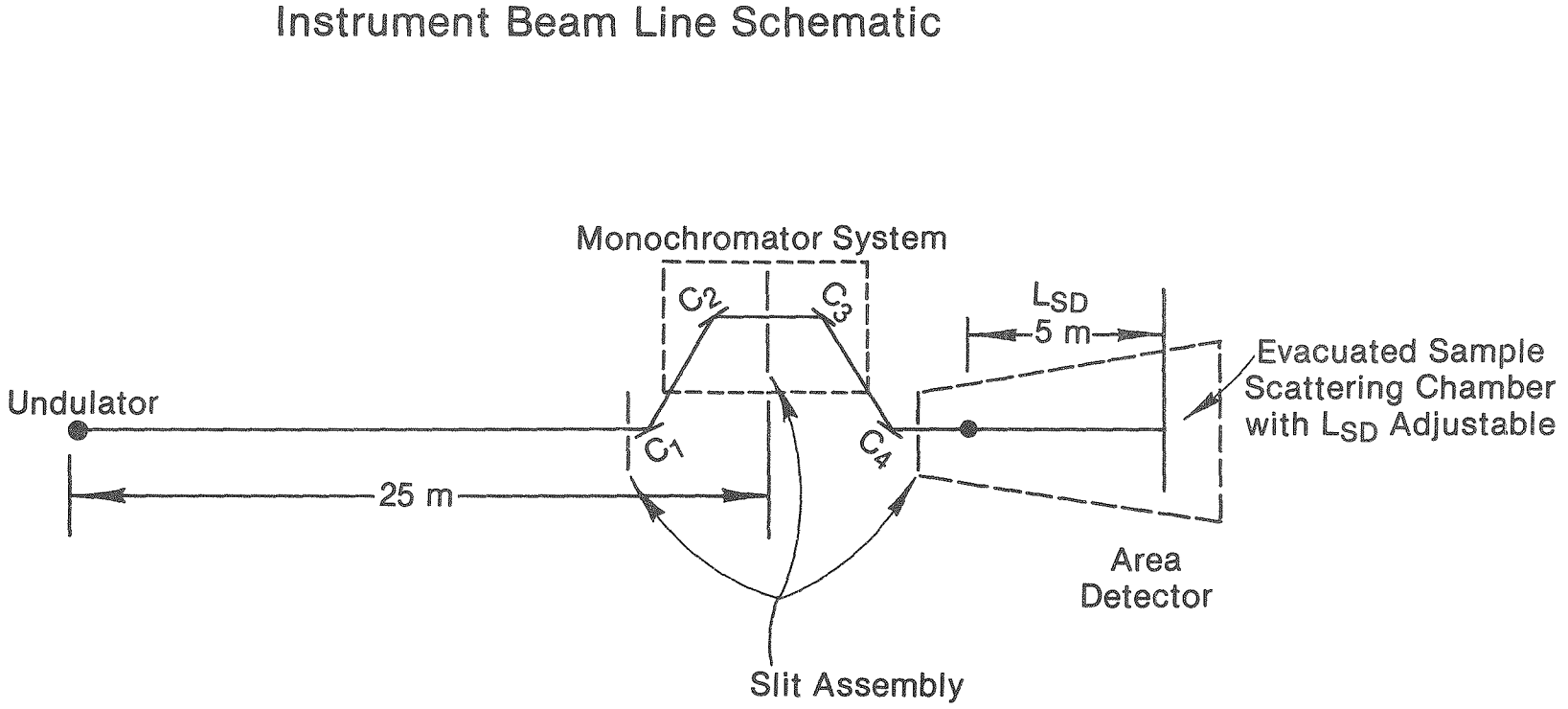

Fig. 7-1 Schematic drawing of the samll-angle scattering beamline

asymmetrically cut crystals, the magnification parameter is defined by

$$m = \frac{\sin \theta_{out}}{\sin \theta_{in}} = \frac{\sin (\theta_B + \alpha)}{\sin (\theta_B - \alpha)} , \qquad (7\text{-}5)$$

where θ_B is the Bragg angle and α is the asymmetric cut angle. The characteristics of the reflected beam from an asymmetrically cut crystal ($\alpha = 11.3°$) for an incident glancing angle (B) of 3°, determined for energies of 5 and 8 keV, are listed below.

E (keV)	m	Linear Footprint Enhancement
5	3	x2
8	12.8	x17

At E = 8 keV, this means that the linear dimension of C1 must be $\geq$ 2.4 cm. From the characteristics of the undulator, we have determined the incident beam to be 0.6 mm wide at 25 m from the source. The output beam from C1 has less angular divergence than the incident beam, but a larger cross-sectional area. In addition, the scattering is dispersive in that wavelength components in the output beam are spatially correlated. The result of choosing a dispersive and asymmetric crystal C1 is to spread the beam profile over a larger surface area, because of heat loads due to the undulator flux on sample. Crystal C2 is also dispersive, but we now choose a demagnifying asymmetric cut to condense the beam size. This crystal must be heated to

produce $d(111)_{C2} = d(111)_{C1}$, since the small sample size (1 mm × 1 mm) demands that the beam not be allowed to drift.

7.4 Estimates of Flux on Sample

To estimate the flux on the sample, we assume the following parameters:

$\Delta E/E = 2 \times 10^{-4}$,

window attenuation $A_w = 0.25$,

monochromator efficiency $R_m = 0.9 \times 4$, and

polarization loss $P_\ell = 0.9 \times 4$.

Then the flux (in ph/sec) is given by

$$f = BR \times \sigma_x \times \sigma_y \times \sigma'_x \times \sigma'_y \times \frac{\Delta E}{E}(\%) \times A_w \times R_m \times P_\ell$$

$$\approx 10^{11} \text{ photons/sec.}$$

7.5 Q Response

We require a 40 mm × 40 mm imaging detector with linear spatial resolution $\delta\ell = 0.25$ mm and a sample-to-detector distance, L_{SD}, of 5 m. The following values are obtained for Q_{min} and δQ at energies of 5 and 8 keV:

E (keV)	Q_{min} ($Å^{-1}$)	δQ ($Å^{-1}$)
5	5×10^{-4}	10^{-4}
8	6×10^{-4}	10^{-4}

For L_{SD} = 0.5 m, we obtain $Q_{min} = 4 \times 10^{-3}$ Å^{-1} and Q_{max}/8 keV = 0.23 Å^{-1} with the detector centered on the incident beam; a higher value of Q_{max} can be achieved by moving the detector off-axis. Several overlapping Q ranges are achieved by adjusting the sample-to-detector distance and by allowing for off-axis positioning of the detector.

7.6 Detector Complement

We have shown that a 40 mm × 40 mm 2-dimensional array can be used, along with variable sample-to-detector distances, to achieve a wide Q range. However, any anticipated anistropy in small angle scattering tends to be important only in the regions of very low to moderate Q. This means that detector additions at $Q \rightarrow Q_{max}$ need not have true 2-dimensional capability. We therefore propose that the area detector be used only in the on-axis configuration and that supplementary annular detectors be used in the high-Q region, as illustrated in Fig. 7-2.

These annular rings could be elements of an imaging detector arranged in such a way as to automatically perform the radial averaging. With the enormous data rates that can be achieved with this instrument, an option for radial averaging provides enormous simplifications in data reduction requirements and is of particular importance in time-resolved experiments. Consider the case of the 40 mm × 40 mm area detector with 0.25-mm spatial resolution. This means that each complete description of I(Q) requires each binned Q value on the detector to results from ~2 pixels, which corresponds to 256 × 256 = 64 K words of data storage. If we choose time-resolved experiments with millisecond resolution (shown to be possible from flux-on-sample estimates), then 10 such time intervals would require 640K words. Radial averaging at large Q significantly reduces the amount of data that must

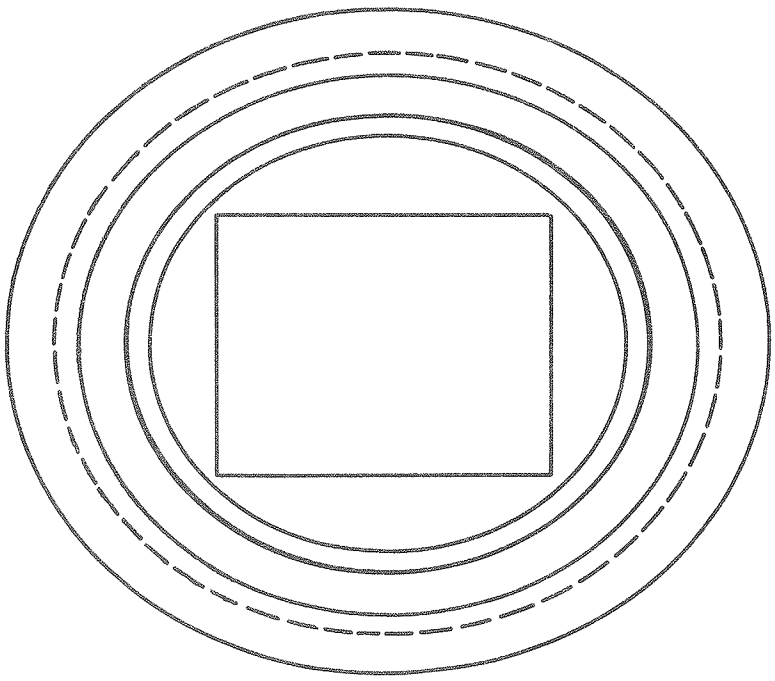

Fig. 7-2 Schematic of annular detector

be treated even during data reduction steps. To produce fundamental quantities like the effective radius of gyration for scattering centers requires as much simplification as can be allowed. Clearly for fast time-resolved studies we require another detector, with buffered linear position-sensitive elements. Fast-readout imaging devices are adequate.

For experiments that require us to focus our attention on very small Q values with very high Q resolution, we propose an alternative point-counting detector that utilizes two Si(111) crystals, as illustrated in Fig. 7-3.

Again, we would use asymmetrically cut crystals with slit systems between the analyzers to enhance Q resolution. Back-reflection geometry for extreme energy resolution is also possible. Step-scanning angular resolution of $\Delta 2\theta = 0.005°$ provides Q resolution consistent with the angular acceptance of the analyzing crystals ($\sim 5\times10^{-5}$ radians), since if $\Delta 2\theta = 5\times10^{-3°}$ then $\Delta\theta = 4\times10^{-5}$ rad.

7.7 Discussion of Q Range

In preceding sections, we have presented the design for an instrument with a very low Q_{min} and a moderate Q range; however, one significant sacrifice was with regard to the tunability of the incident-beam energy. This problem is circumuented by using a low-E_c wiggler which provides a white spectrum. In the following sections, we propose a second diffractometer designed to make use of the inherent advantages of tuning the incident energy. Note from Eq. (7-4) that if we can adjust the scattering contrast associated with $(\rho_p - \rho_m)$, then we have unique information that cannot be established with any other experiment. Differential measurements, taken above and below the absorption edges of constituent atoms in a multi-atom scattering sample, can be used to gain information on the conformation and the

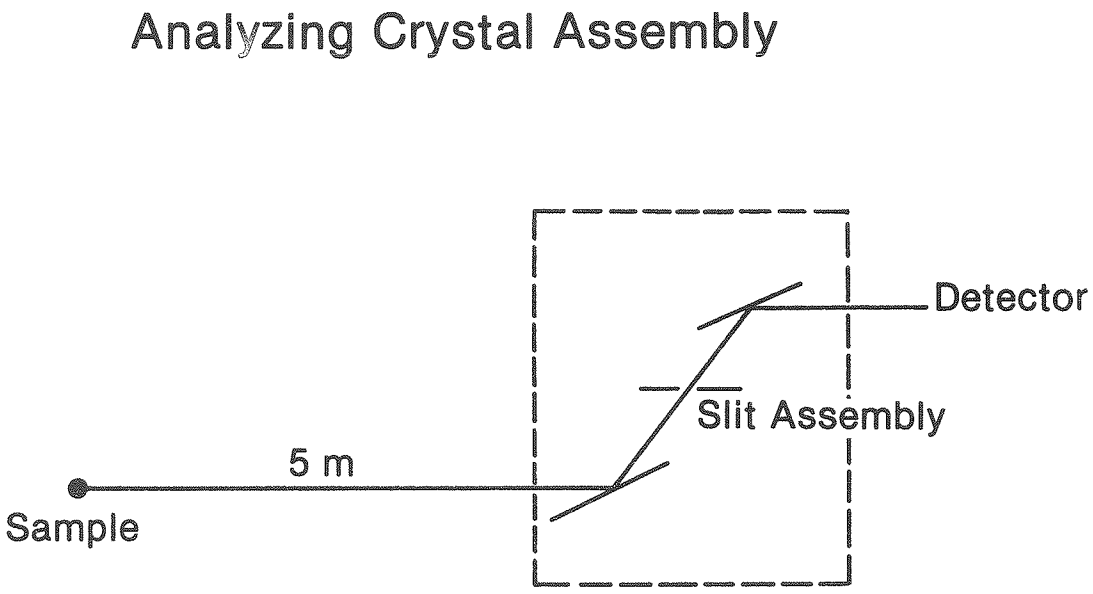

Fig. 7-3 Schematic of double-crystal point-counting detector

state of aggregation of atoms. Using these anomalous scattering techniques, we can obtain information about atoms located next to each other in the Periodic Table. For example, we could study the scattering associated with precipitates in a Cu-Zn alloy.

7.8 Design of an Anomalous-Dispersion Small Angle Diffraction Instrument

The design of this moderately low-Q machine is very similar to that presented above, except that a wiggler is used as the insertion device. In fact, with an undulator and wiggler mounted on a carousel, only one beamline is required.

7.9 Wiggler

Since we desire photon energy in the range 8 keV $\leq$ E $\leq$ 30 keV, we choose a low-field wiggler with the following characteristics: E_c = 10 keV, K = 9, G = 11 cm, N = 40, and period = 25 cm. With this design, we can achieve a source flux, f, with the following range:

$$4 \times 10^{14} \leq f \leq 10^{14} \text{ (photons/sec/0.1\%BW/mrad } \theta)$$

over the energy range 8 $\leq$ E $\leq$ 30 keV, with $\theta \sim 2$ mrad and $2\psi \sim 0.2$ mrad. The wiggler parameters chosen above provide a convenient high-energy cut-off. For E $\sim$ 40 keV, the flux should be several orders of magnitude lower than the values given above. For E > 15-20 keV, intrinsic harmonic-free operation can be realized. The low-energy components in the beam are attenuated with filters in the front end.

7.10 Monochromator Assembly

To maintain compatibility with the undulator instrument, we choose a four-crystal design as illustrated in Fig. 7-4, where C5 and C6 are asymmetrically cut crystals. In addition, C6 must be sagitally focused to account for the horizontal beam divergence. Monochromator crystals C7 and C8 could be multilayer structures if available, or Ge(111) symmetrically cut crystals.

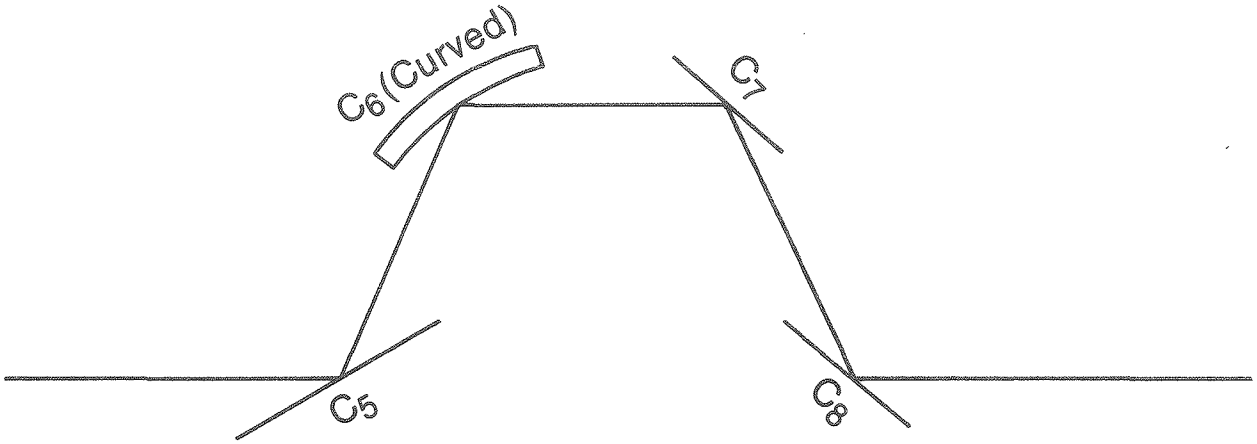

Monochromator Assembly for Wiggler

Fig. 7-4 Monochromator assembly for wiggler

8 General-Purpose Scattering for Materials Studies

8.1 Introduction

The proposed beamline aims to provide enhanced capabilities for a wide variety of experiments, rather than being optimized for a narrow class of experiments. This does not mean that it is a compromise to serve a variety of needs. Rather, many scientific problems have been identified which can be investigated optimally on the proposed beamline. They include diffuse scattering from a single crystal and polycrystalline specimens; high-resolution powder diffraction at high temperatures and pressures; anomalous scattering from single-crystal, powder, and amorphous specimens; and weak scattering phenomena, such as charge density waves and diffraction from free liquid surfaces, which require a high-flux, spectrally pure tunable beam. These research areas constitute a sizable fraction of the total research effort in materials science and it is appropriate that a national user facility should provide near-optimum, state-of-the-art capabilities for carrying out such experiments.

8.2 Performance Requirements

In order to achieve its stated purpose, the proposed beamline meets the following requirements:

1. The photon energy is continuously tunable between 5 and 30 keV.

2. The energy resolution is around 2-5eV across the energy range; it can be improved by sacrificing flux or changing monochromator crystals.

3. The flux on sample is high, approaching 10^{14} ph/sec at 10 keV.

4. The monochromatic beam is clean, with harmonic contamination of one part in 10^5 or less.

5. The photon source is chosen for high flux in the selected energy range, but the total power in the beam is kept moderate to facilitate x-ray optics design. This requires a source with critical energy around 10 keV, which has the added benefit that the high-energy photon content of the beam is small.

6. The monochromatic beam can be focused down to 0.1 mm x 0.4 mm on the sample, if desired, with a divergence of 0.2 mrad x 1.5 mrad. Alternatively, by defocusing the vertical size to 2 mm, one can improve the vertical divergence by one order of magnitude.

7. The scattering instrument is capable of both single-crystal and powder work, is able to reach low and high scattering angles (-30° to 170°), and is sturdy enough to carry heavy attachments, such as cryostats, analyzing crystals, furnaces, UHV systems, and high pressure cells, all of which should be available.

In order to meet these performance requirements, the configuration described in the next few paragraphs was decided upon. The design philosophy was to keep components as straightforward and flexible as possible. In most cases, designs already tried and proved at existing synchrotron installations have been adopted.

8.3 Photon Source

The selected photon source is a 40-pole wiggler designed with a low critical energy (E_c) of 9.6 keV, which provides high flux at a moderate total power. Its characteristics are given in Table 8.1 (Case A). The choice of E_c = 9.6 keV is near-optimum for minimizing unwanted high-energy photons, which are difficult to eliminate without compromising the flexibility of the monochromator optics.

It is also possible to design this wiggler with a variable gap (still comfortably large) which allows an increase in E_c to 15-20 keV. Reducing the gap from 11 cm to 8 cm (see Table 8-1, Case C) increases E_c to 17 keV. Unfortunately, the power density doubles and the total power quadruples in this situation. One can, however, resort to a variety of procedures to make the heat problems more manageable. First, the wiggler will be operated in this mode when photon energies in excess of 25 keV are desired. Carbon filters can then be used in the white beam to absorb approximately half the power without significantly affecting the high-energy photon flux. Also, at such high energies, the angle of incidence on the first monochromator crystal is such that the beam spreads by a factor of ten compared to normal incidence.

8.4 Monochromator Optics

A fairly simple design (Fig. 8-1) is proposed for monochromatizing and focusing the wiggler beam. This design borrows heavily from the experience at NSLS beamlines X-14, X-18, and X-19. The monochromator will be a double Si(111) arrangement, with the first crystal flat and cooled and the second ribbed and elastically bent to focus in the sagittal direction. It is anticipated that standard cooling techniques will be adequate to handle the 1.8-kW total heat load, as well as the 7 W/mm^2 peak specific load at normal

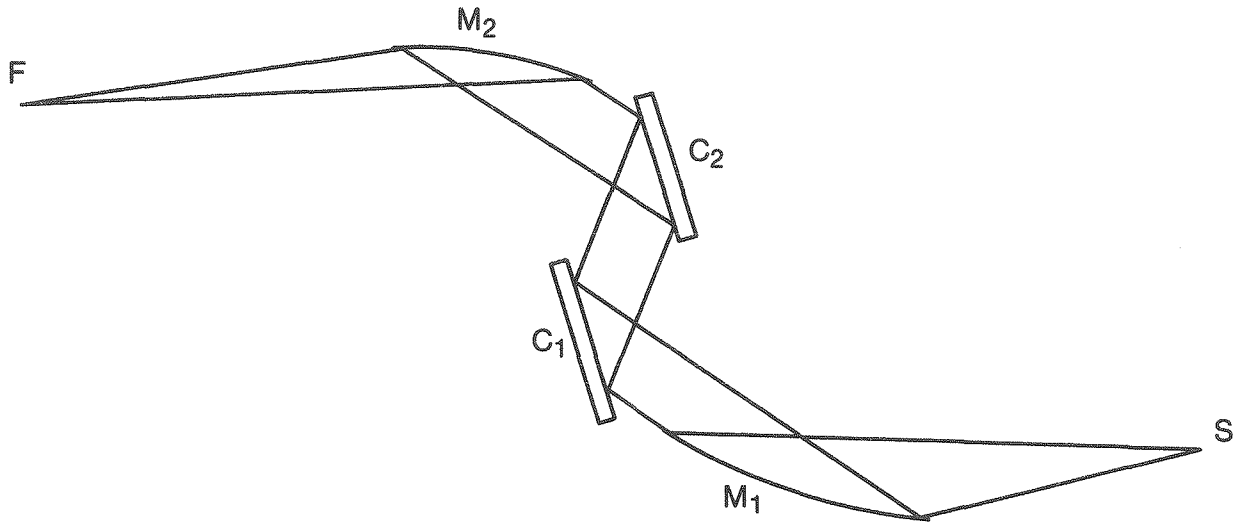

Proposed Monochromator Layout

S – Source

M_1 – First Mirror (Cooled)

C_1 – First Crystal (Flat Si (III) Cooled)

C_2 – Second Crystal (Curved, Ribbed Si (III))

M_2 – Second Mirror

F – Focus

Mirror Angles Shown Greatly Exagerated

Fig. 8-1 A schematic diagram of the monochromator showing the bent mirrors and Si(111) crystal pair

incidence at the design distance of 40 m. Such levels of power and power density are successfully being handled now at both CHESS and SSRL. This monochromator design has been working very satisfactorily in a number of beamlines at NSLS (although the cooling requirements there are less stringent).

For low-energy applications (E < 15 keV), mirrors become necessary for harmonics rejection. Mirrors are also necessary at all energies if focusing of the beam in the vertical direction is desired. This proposal includes mirrors both upstream and downstream from the monochromator. Either one or both of the mirrors can be moved out of the beam. The upstream mirror will undoubtedly require cooling, but this does not present special problems, since most of the incident power is reflected and the fraction absorbed is spread over a large area. The power density will be at most a few W/cm^2.

The mirrors will be initially fabricated flat and then bent elastically to the desired radius. In the interests of ease of fabrication and cooling efficiency, the mirrors will be metallic. An aluminum mirror of the design proposed here has been in service at NSLS (on beamline X-14) with good results. Its mechanical performance (bending, stability) has been excellent, although its surface finish needs improvement. It is expected that as experience accumulates at existing synchrotron sources over the next one or two years, superior mirrors will become available.

A two-mirror arrangement such as described above provides a non-compromise solution for best achievable energy resolution and focusing with no sacrifice in flux, provided mirrors with good surfaces can be fabricated. Such an arrangement is presently being installed in the X-19 lines at NSLS. The first mirror is bent to produce a parallel beam (i.e., it focuses at infinity). This allows the monochromator to achieve the energy resolution

dictated by its rocking curve width, rather than the synchrotron radiation opening angle (which is three times larger than even the rocking curve width of Si(111)). The second mirror then focuses the beam down to a size equal to the source size (0.1 mm) at the specimen.

Table 8-1

Parameters of a Variable-Gap Wigglers

	Case A	Case B	Case C
Magnet Gap (cm)	11.0	9.0	8.0
Period (cm)	25.0	25.0	25.0
B_o (T)	0.40	.56	.70
Peak K.	9.3	13	16.4
No. of Poles	40	40	40
Wiggler Length (m)	5.0	5.0	5.0
E_c (keV)	9.6	13.4	16.8
Total Power (kW)	1.8	3.6	5.6
Width of Distribution in Vertical Direction (mrad)	0.19	0.19	0.19
Maximum Width of Distribution in Horizontal Direction (mrad)	1.6	2.2	2.8
Peak Power (kW/mrad θ)	1.5	2.1	2.6
Peak Power (kW/mrad^2)	11.2	15.6	19.5
Power at Normal Incidence at 40 m (W/mm^2)	7.0	9.8	12.2
Flux at E_c (10^{14} ph/sec/0.1%BW/mrad θ)	3.8	3.8	3.8

9 Multiple Energy Anomalous Dispersion Studies of Proteins

9.1 Introduction

We propose to build a protein crystallography beamline on a wiggler insertion device of the 6 GeV Light Source. This will be used to measure multiple energy anomalous dispersion (MEAD) from protein crystals; it can also be used to collect routine diffraction measurements. It is designed to use both very small (0.010 mm maximum linear dimension) and standard (0.1-0.5 mm) crystalline samples, and to produce completed, reduced data from these crystals in short (hours or days) periods of time (hours or days).

Protein crystallography allows the precise determination of atomic structures of large biological molecules, which makes possible both an understanding of their function and the prospect of modifying protein structures to improve their economic value. On conventional x-ray sources, data collection from routine crystals requires weeks to months; on existing synchrotron sources, it can be completed in a few days.

Multiple-energy anomalous dispersion (MEAD) from heavy atoms within a protein crystal (e.g., naturally occurring zinc or copper in some enzymes; iron in heme-containing proteins; artifically inserted rare-earths or uranium holds promise as a means to determine directly the structure factor phases from the 10^4 or 10^5 Bragg reflections typical of protein crystallography, eliminating the need for the isomorphous replacement phasing method. In essence, one must record the Friedel pair intensities at three or more wavelengths: at the absorption edge and at points well above and well below the edge. Analysis of the intensity changes as functions of energy can yield accurate phase information in an analytical way, without requiring an initial guess as to the location of the heavy atom and its accurate refinement by the least-squares method.

An existing facility at SSRL for anomalous-dispersion measurements has too low an intensity to be conveniently used. The proposed 6 GeV wiggler source for MEAD will have sufficiently high intensity, while maintaining a sufficiently good energy resolution, to successfully and conveniently perform these valuable phasing experiments. With a fast, accurate detector, data collection on this beamline for a typical protein crystal should require only a few minutes of user time, and a few hours of computer CPU time. We have integrated our design for the beam intensity, sample crystal behavior, and detector characteristics to produce a beamline that provides convenient and fast data collection even on reasonably small samples. Some parameters of the MEAD beamline are given in Table 9-1.

Table 9-1

Parameters of Multiple-Energy Anomalous-Dispersion Beamline

Beam Energy, E (keV)	8-20
Energy Resolution, $\Delta E/E$, where $\Delta E \sim 1$ eV	1×10^{-4}
Incident Intensity of Sample, I_o (sec^{-1})	4×10^{13}
Linear Absorption Coefficient of Sample, μ (cm^{-1})	0.7-0.04

9.2 Sample Lifetime

As discussed elsewhere,[1] the lifetime T_d of a protein crystal in a synchrotron beam is

$$T_d = \frac{N_s}{I_o d^3 \mu e},$$

where I_o is incident intensity; d is the linear sample dimension in mm; γ is the linear absorption coefficient; e is the "damage factor," i.e., the number of protein molecules destroyed per absorbed quantum; and N_s is the number of protein molecules in the crystal. This can be shown to reduce to

$$T_d = (I_o \lambda^2)^{-1}.$$

The sample lifetime T_d has been calculated for typical samples exposed to beam energies of 8 and 20 keV. As shown in Table 9-2, samples lifetime is independent of sample size and varies from 14 to 250 sec for the example considered.

Table 9-2

Calculated Samples Parameters for Two Beam Energies and Two Linear Samples Dimensions

	d(mm)	
	0.25	0.01
Heat Absorbed (W/sec) at		
8 keV	5.6×10^{-4}	3.6×10^{-8}
20 keV	0.8×10^{-4}	0.5×10^{-8}
Temperature Rise (deg/sec) at		
8 keV	8.5	8.5
20 keV	1.2	1.2
Sample Lifetime (sec) at		
8 keV	14[a]	14[a]
20 keV	250[b]	250[b]

[a] 36/e where e = 2.5.
[b] 625/e where e = 2.5.

The time T_r needed to record useful data, is given by[2] to relate

$$T_r = (I_o d^3 \lambda^2)^{-1},$$

so the ratio of recording time to damage time is

$$T_r/T_d = d^3$$

and is independent of both λ and I_o. As long as two criteria are met, it is not essential to increase the speed of data collection; the experimental statistics will depend only on the sample size. These two criteria are as follows: (1) the data must be collected before time-dependent decay processes destroy the sample, within about i.e., 1-10 minutes; and (2) the detector must be capable of accurately recording the diffracted x-rays.

9.3 Description of the Detector

The protein crystallography detector is described in the 6 GeV Light Source proposal (ANL-86-8). It is capable of recording 10^{10} photons/sec in the energy range from 8 to 25 keV with 0.15% precision, on a 512x512 pixel surface, with 0.5 quantum detector efficiency. The frame readout rate will be 1.25 seconds, and we assume that the frame can be recorded in a time period between 0.1 and 1.0 seconds, so the duty cycle on the protein crystal will be such that between 10% and 50% of the experimental time is spent actually irradiating the sample.

Because several measurements must be taken of each Bragg reflection, each at a separate energy, and a crystal may not survive the entire set of measurements, these experiments may require more than one crystal to

complete. The major limiting feature of the current experiment design is the detector speed, which very likely can be accelerated by technological improvements during the next 5 years. We need about a factor of 10 increase in detector speed to allow complete data collection from a single crystal. As currently configured, these experiments require 4-10 crystals each, a number consistent with the usual data collection conditions for isomorphous replacement phasing (data collection on rhinovirus crystals at the CHESS synchrotron in 1984 required about 100 crystals).

9.4 Description of the Wiggler Beamline

A schematic drawing of the MEAD beamline appears in Fig. 9-1. The photon source for the beamline is a low-energy wiggler with a critical energy of 9.6 keV. The flux at 12 keV for this wiggler is 3.2×10^{14} photons/ 0.1%BW/sec/mrad θ. With the appropriate photon optics, it is estimated that this source will provide 4×10^{13} photons with an energy of 12 keV on an experimental stage 0.5 mm x 0.5 mm in size. The photon optics consist of the (111) planes of two Si crystals. The first crystal is flat. This crystal provides the primary energy resolution for the experiment and absorbs most of the heat in the photon beam. The second crystal sharpens the bandwidth of the photon beam and is bent perpendicular to the beam to provide sagittal focusing. A curved mirror downstream from the two crystal elements focuses the beam in the vertical direction. The beamline energy can be tuned from 8 keV to 20 keV by rotating the first crystal and by both rotating the second crystal and moving it along the exit photon beam direction. Both the vertical and horizontal dimensions of the beam at the first crystal element are controlled by collimators. These collimators control both the energy bandwidth and the intensity of the beam at the experimental stage. The photon

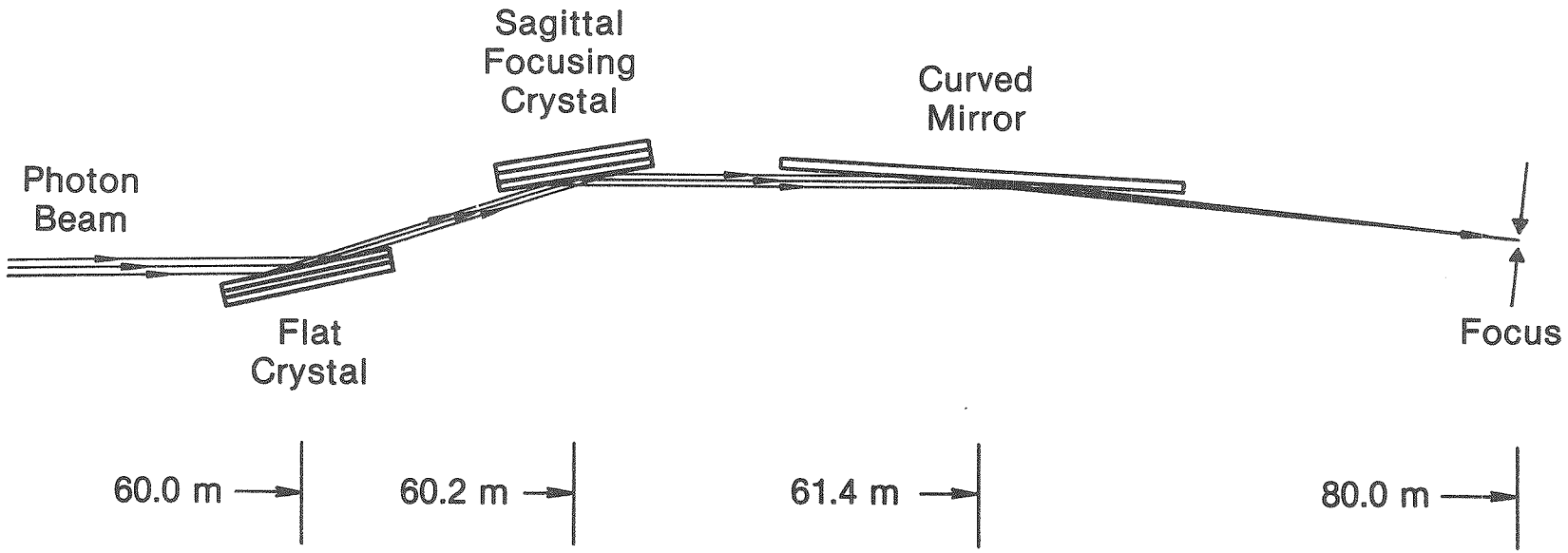

Fig. 9-1 Schematic drawing of the beamline for multiple-energy anomalous studies of proteins

beam at the first crystal element has a vertical opening angle of 0.2 mrad and a horizontal opening angle of 2 mrad with the control collimators at full open. This results in a beam that is 1.2 cm high and 12 cm wide at the first crystal. The footprint of the beam on this crystal is 12 cm wide and 7.5 cm in the direction of the beam. The maximum thermal load at the center of the footprint will be 50 W/cm. This heat load will require the first crystal to be strongly cooled. Consideration is being given to using liquid gallium with a channel-cut crystal to give an effective crystal thickness of 3 mm and a maximum temperature rise of 11.5° at the center and 7.0° at the lateral edge of the beam. The second crystal is located 20 cm downstream from the first and has a similar footprint but very much less thermal heating. The focusing mirror is 120 cm farther downstream and is mounted at an angle of 6 mrad to the beam. This requires a platinum-coated mirror that is 200 cm long with a radius of curvature of 4730 m. A flux of 4×10^{13} photons/sec on the experimental stage is expected for the case where the horizontal width of the beam is stopped down to one half of the maximum allowable. The parameters of the optical elements are summarized in Table 9-3.

With the vertical collimator fully open (0.2 mrad), $\Delta E/E$ for the beam at 12 keV is 0.6×10^{-3} ($\Delta E = 7.2$ eV). The angular divergence in the vertical direction is 0.6 mrad (2 min of arc). The angular divergence in the horizontal direction is 3.0 mrad. For some applications of the beamline, this divergence is too large and a fourth optical element is needed to make the beam more parallel at the experimental stage. This element is a small mirror, curved perpendicular to the beam and located about 2 m from the stage.

Table 9-3

Parameters of the X-Ray Optics for the Multiple-Energy Anomalous Dispersion Beamline

	1st Crystal	2nd Crystal	Mirror
Material	Si	Si	Pt coated
Crystal Planes	(111)	(111)	Curved
Shape	Flat	Curved ($\perp$ to beam)	Curved ($\parallel$ to beam)
γ Energy (keV)	12.0	12.0	12.0
Incident Angle (deg)	9.486	9.486	0.3438
Incident Angle (rad)	0.1648	0.1648	6×10^{-3}
Radius of Curvature (m)	-	-	4730
Distance from Source (m)	60.0	60.0	61.4
Vertical Heights, Δy (cm)	1.2	1.2	1.2
Horizontal Width, Δz (cm)	6.0*	6.0*	6.1[a]
Horizontal Length, Δz (cm)	7.3	7.3	200.
Peak Power (W/cm)	50.0	5×10^{-5}	-
Maximum $\Delta T/\Delta \ell$, (°C/cm)[b]	11.5	-	-

[a] Collimated down to 1 mrad in the horizontal direction.
[b] ℓ = length into monochromator crystal.

REFERENCES

1. J. R. Helliwell and R. Fourme, ESRP Internal Report IRI 4/83 (1983).

2. U. W. Arndt, J. Appl. Crystallogr. 17, 118 (1984).

10 Protein Crystallography

10.1 Introduction

We propose to build a protein crystallography beamline on a bending magnet of the 6 GeV Light Source. This beamline will be used to make conventional diffraction measurements. The beamline is designed to use both very small (0.020 mm maximum linear dimension) and standard (0.1-0.5 mm) crystalline samples, and to produce completed, reduced data from these crystals in short periods of time (hours or days).

Protein crystallography allows the precise determination of atomic structures of large biological molecules, which makes possible both an understanding of their function and the prospect of modifying protein structures to improve their economic value. On conventional x-ray sources, data collection from routine crystals requires weeks to months; on existing synchrotron sources, it can be completed in a few days. However, these data are currently collected by film, and film processing typically requires weeks. Thus, development of an effective electronic multielement detector covering many square centimeters of area is a necessary and implicit component of the design of our protein crystallography beamline. With a fast, accurate detector, data collection for a typical protein crystal on a bending-magnet beamline at the 6 GeV Light Source should require only a few minutes of user time, and a few hours of computer CPU time. We have integrated our design for the beam intensity, sample crystal behavior, and detector characteristics to produce a beamline that provides convenient and fast data collection even on reasonably small samples.

Some parameters of the protein crystallography beamline are given in Table 10-1; the detector is the same as that discussed in Section 9.3.

Table 10-1

Parameters of Protein Crystallography Beamline

Beam Energy, E (keV)	12
Incident Intensity on Sample, I_o (sec^{-1})	2×10^{12}
Linear Absorption Coefficient of Sample, u (cm^{-1})	0.2

10.2 Sample Lifetime

The lifetimes of typical samples with linear dimensions d = 0.25 and 0.02 mm, respectively, have been calculated as in Section 9.2. The results are shown in Table 10-2.

Table 10-2

Calculated Sample Parameters for Two Linear Sample Dimensions

Heat Absorbed (W/sec) at	
d = 0.25 mm	1.2×10^{-5}
d = 0.02 mm	6×10^{-9}
Temperature Rise (deg/sec)	0.18
Lifetime (sec)	1000

[a] 2500/e where e = 2.5.

Assuming that the damage factor e is less than 10, crystals should survive about 15 minutes of uninterrupted beam exposure. Since we have designed the

detector to record an entire 3-dimensional data set within 10 to 200 seconds of actual beam exposure, our apparatus should be capable of recording excellent protein diffration data.

10.3 Description of the Beamline

The layout of the protein crystallography beamline is the same as that shown in Fig. 9-1. The photon source is a bending magnet with a critical energy of 19 keV. With the appropriate photon optics, it is estimated that this source wil provide 2×10^{12} photons with an energy of 12 keV on the experimental stage 0.5 mm x 0.5 mm in size. The photon optics are the same as for the MEAD beamline described in Section 9. The maximum thermal load at the center of the beam footprint on the first crystal will be 13.6 W/cm. As in the case of the MEAD beamline, this heat load will require the first crystal to be strongly cooled. Consideration is being given to using liquid gallium with a channel-cut crystal to give an effective crystal thickness of 5 mm and a maximum temperature rise of 5.2°. A flux of 2×10^{12} photons/sec on the experimental stage is expected for the case where the horizontal width of the beam is stopped to one half of the maximum allowable. The parameters of the optical elements are the same as for the MEAD beamline (Table 9-3), except for the peak power at the first and second crystals (14.2 and 1.4×10^{-5} W/cm^2), respectively) and the maximum $\Delta T/\Delta \ell$ at the first crystal (5.4°C/cm).

11 Time and Space Resolved X-Ray Spectroscopy

11.1 Introduction

Conventional EXAFS spectroscopy has proved to be a valuable tool in studies of chemical and biological systems and of materials, but it has been limited to studies of rather large areas (governed by beam size); the minimum practical area has been ~ 0.1 mm x 0.1 mm. Intensity scales directly with area, so large sacrifices in intensity must be made to study smaller areas. The situation is further worsened by the fact that any beam inhomogeneities caused by mechanical instabilities of the beamline optics can severely distort a serially acquired EXAFS spectrum. Further, because serially acquired EXAFS spectra take many minutes to obtain, short-time-domain experiments (e.g., on kinetics, phase transformations, or melting phenomena) have not been possible.

In principle, it is most advantageous to use energy-dispersive focused-beam EXAFS optics to perform either highly localized or very fast x-ray absorption spectroscopy experiments. In this dispersive mode, a sheet of synchrotron radiation is collected by a bent crystal, focused to a point, and redispersed beyond the focal point, and intensities of the spatially resolved energy spectrum are recorded by a one-dimensional position-sensitive detector. Since there are no moving parts, there are no mechanically induced spectral inhomogeneities; since an entire spectrum is collected simultaneously, any losses in intensity due to small area or short times are recovered.

A spectrometer with the specifications listed in Table 11-1, equipped with pinhole collimators to limit beam size to the order of 20 μm, makes feasible a number of experiments on previously inaccessible systems.

Table 11-1

Design Goals for Energy-Dispersive X-Ray Spectrometer

Dynamic Energy Range	5.5-23.3 keV
Dynamic Temporal Range	~ 100 nsec ("one-shot") to ∞[a]
Dynamic Spatial Range	~ 100 μm^2-4 mm^2
Energy Scan Range	Variable
Energy Resolution Range at 10 keV	$\geq$ 1 eV

[a]Detector framing rate = 140 μsec.

These include time-resolved EXAFS experiments as well as high-spatial-resolution experiments valuable to materials science, geosciences, atomic and molecular physics, and surface science.

The spectrometer could be used in any one of three principal modes. In a simple time-resolved mode, the entire focused beam is transmitted through the sample and collected by the position-sensitive detector. The proposed detector has a time resolution of about 140 μsec, which is sufficient for establishing the kinetics of many biological reactions. To increase temporal resolution, high-speed chopping wheels can be employed; however, the best temporal resolution can be obtained (for XANES experiments) in so-called "one-shot" experiments with only a single pulse of radiation of 100-nsec duration from a single bunch of positrons; the positron bunch frequency of 2.67 μsec dictates the maximum time slices in the "one-bunch" mode. Thus, this facility provides the means for studying many types of time-dependent phenomena, such as biological and chemical kinetics, phase transformations, and melting/annealing phenomena.

A second, high-spatial-resolution mode would be important in studies of microcrystalline metastable and compositionally graded amorphous materials, geological samples, and atomic or molecular beams. Crystalline metastable phase alloys prepared by co-deposition cannot be studied by conventional EXAFS, since the single-phase regions are small; sometimes it would be desirable to study a single grain. In compositionally graded amorphous alloys, the spatial resolution must be much smaller than the distance over which compositional variations occur. In thin rock sections, it is necessary to have high spatial resolution since most geological samples are complex multiphase systems. In atomic or molecular beam experiments, in which beams of particles are either collided or excited by another source of radiation, high spatial resolution is necessary to map out the products of the collisions or the excitations.

Finally, the spectrometer could operate in a glancing-angle/external- reflection mode. In this so-called total-reflection EXAFS ("REFLEXAFS") mode, the focused incoming radiation impinges on a flat sample at a glancing angle, and the reflected redispersed beam collected by the position-sensitive detector reveals changes in reflectivity due to absorption. This technique can be used to study surfaces, monolayers, or even interfacial structures; it combines the advantages of signal enhancement from the surface and the parallel detection mode to cut counting time and ensure spatial registry with the sample. Work by Fontaine and co-workers at L.U.R.E. has already demonstrated the feasibility and value of REFLEXAFS in the study of surfaces, monolayers, and buried interfaces.

11.2 Description of Beamline

These x-ray absorption measurements and related ones are feasible only on a high-brightness source, such as the proposed 6 GeV Light Source. According to the design specifications described in Ref. 1, a bending-magnet source is best for this application, since the small size (82 μm vertical x 212 μm horizontal) and angular divergence (5 μrad vertical x 89 μrad horizontal) of a bending-magnet source allow more photons to pass through a focal point than is the case for other sources with higher emittance. The entire beam delivery system from the ring to the monochromator should be a UHV stainless steel system to eliminate ozone production, scattered radiation, and carbon contaminants on optical components. Spatial requirements are larger than in conventional EXAFS, since focusing distances (monochromator to sample, sample to detector) are on the order of meters, and the angular range is from nearly 0° to nearly 45°. To accommodate these requirements, the total hutch size is approximately 5 m x 6 m.

Figure 11-1 shows a conceptual layout of an energy-dispersive x-ray spectrometer for the proposed 6 GeV machine. The beamline itself is separated from the ring by a water-cooled beryllium window. This window both separates ring and beamline vacuum and eliminates the lower energy components of the synchrotron spectrum to reduce heat loads on downstream optical components. Downstream from movable beam-definition slits, the first optical component will be a water-cooled, rhodium-coated flat silicon carbide mirror (to reject higher harmonics), followed by a dynamically bent collimating/focusing mirror. Placing the first mirror at 15 m from the source results in a worst-case heat loading of ~2.5 W/cm^2 on the central square centimeter of the mirror; this low heat load can easily be accommodated by current water-cooling technologies. In addition, since the 15-m mark is well within the shield

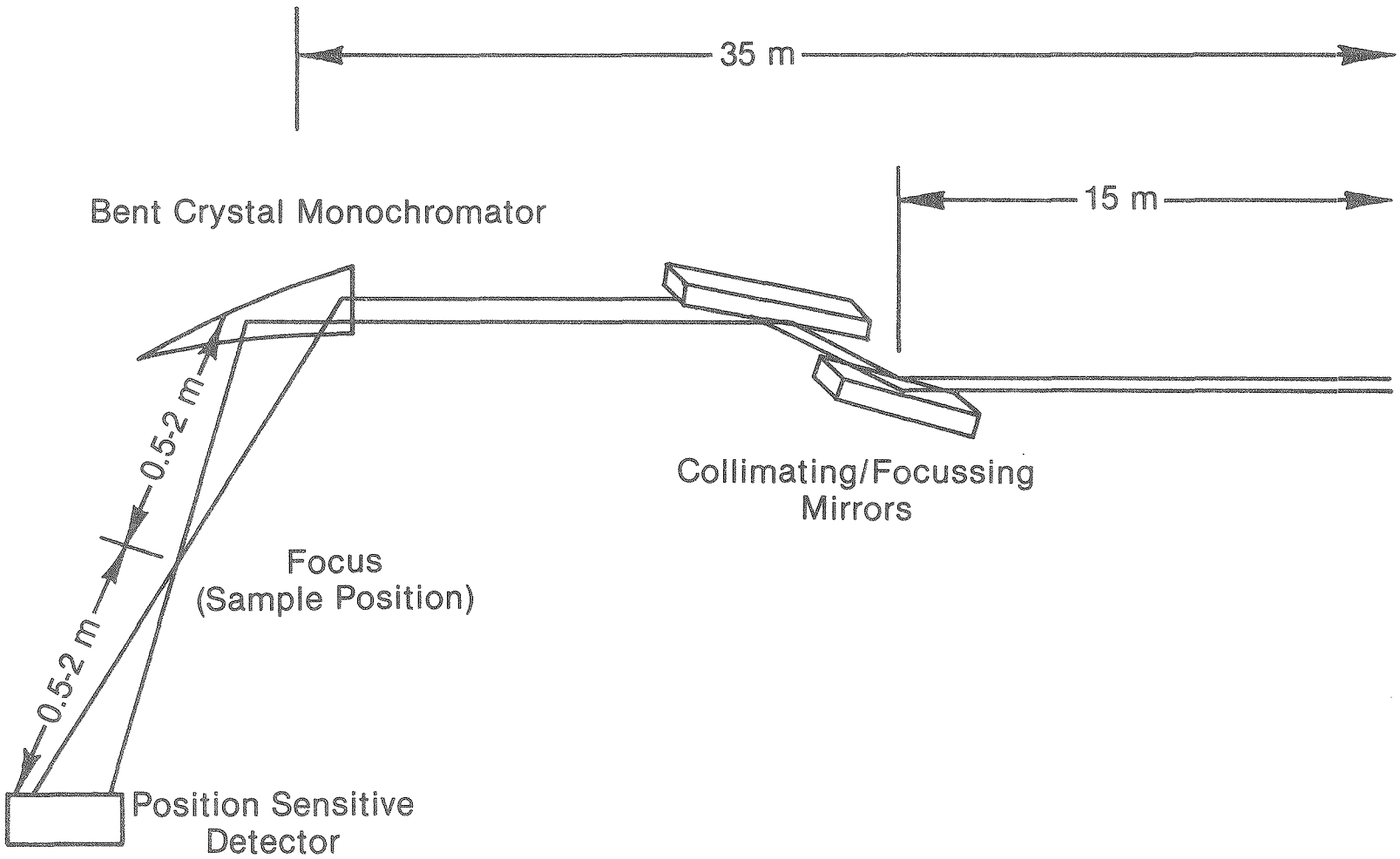

Fig. 11-1 Conceptual layout of energy-dispersive beamline

wall, the amount of high-energy radiation scattered in the experimental hall is minimized. The second dynamically bent mirror, based on the successful ORNL-BNL design currently in use at the NSLS on beamline X-14, can be used to either collimate the beam or focus it at the sample.

Optical calculations for an energy-dispersive crystal monochromator have dictated optimum design parameters. We define R = bending radius of the crystal, P = distance from source to crystal, P' = distance from crystal to focus (sample), P'' = distance from focus to detector, and ℓ = length of crystal subtended by the synchrotron radiation. θ is the Bragg angle of the crystal (optical) center, and ΔE (= 1 keV) is the nominal width of an EXAFS spectrum. Figure 11-2 shows the geometric layout of the monochromator. The curves in Fig. 11-3 show bending radii for Si(111) crystals as a function of photon energy, for three values of P'. All these bends are possible without damage to the crystals or degradation of rocking curves.

The length of the synchrotron radiation footprint on the crystal is a serious design consideration. Figure 11-4 shows crystal length as a function of energy for three values of P'. It is evident that for soft x-rays, P' must be limited to ~ 0.5 m; otherwise, the crystal becomes impractically long and the beam width normal to its propagation axis becomes too wide for practical use. To satisfy these concerns, we set as a design parameter a horizontal opening angle of about 3.5 mrad with a source-to-monochromator distance of 35 m.

The monochromator itself consists of a cooled triangular-cut crystal with drives for θ, x translation (normal to beam axis), crystal curvature, and tilt. All motions can be realized via linear feedthroughs to simplify design and maximize UHV integrity. A wide-angle-range, differentially pumped Be window separates the monochromator from downstream components, and thus

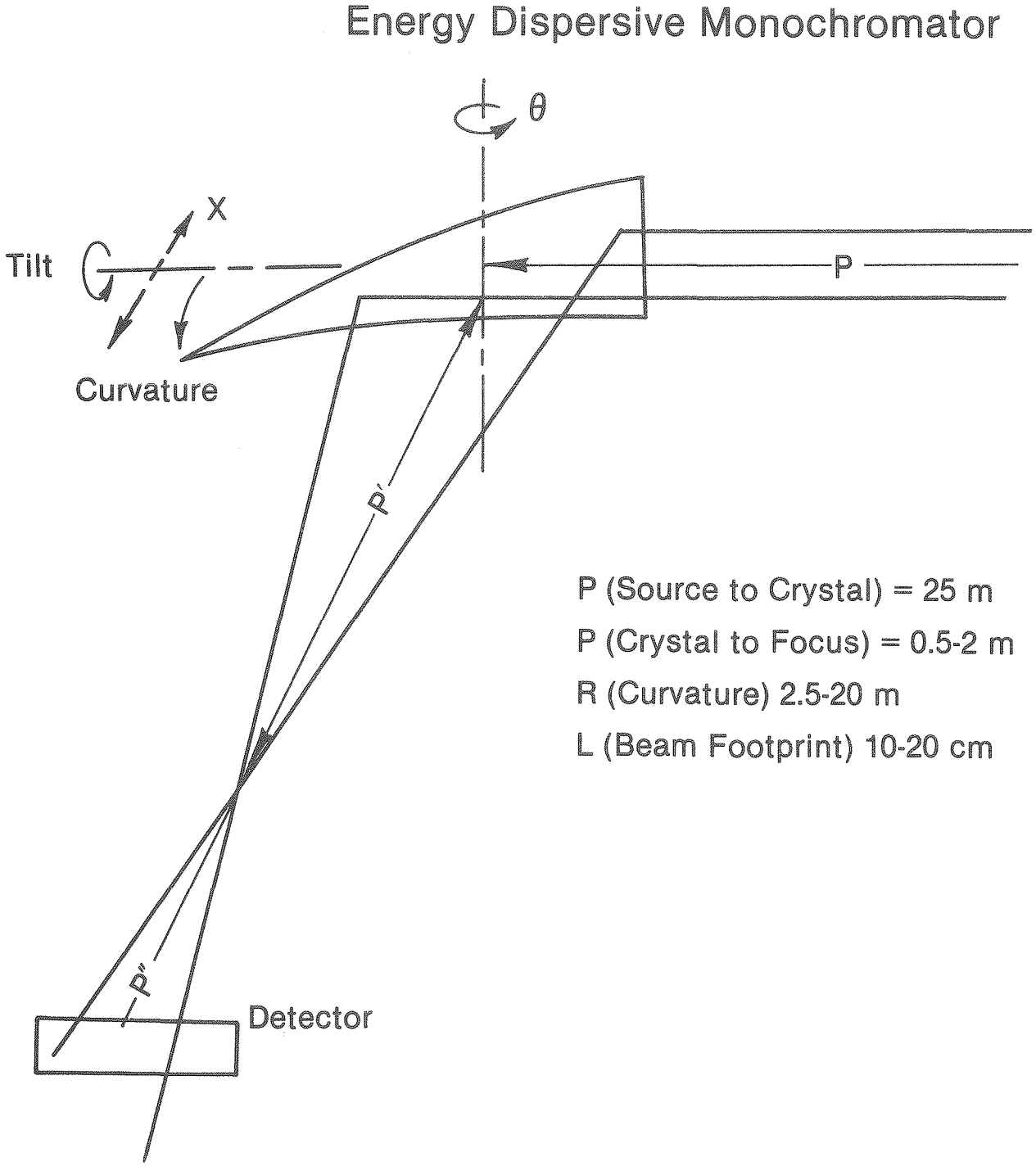

Fig. 11-2 Geometric layout of energy-dispersive monochromator

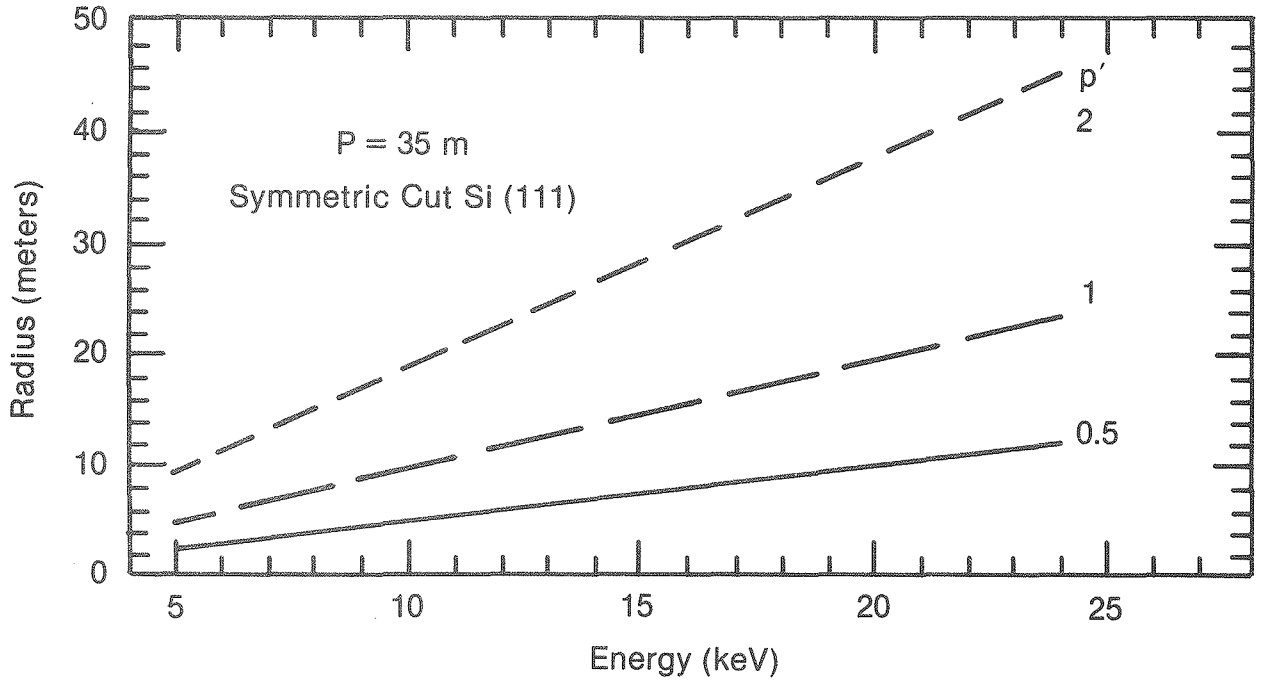

Fig. 11-3 Bending radii for Si(111) crystals with various values of P'

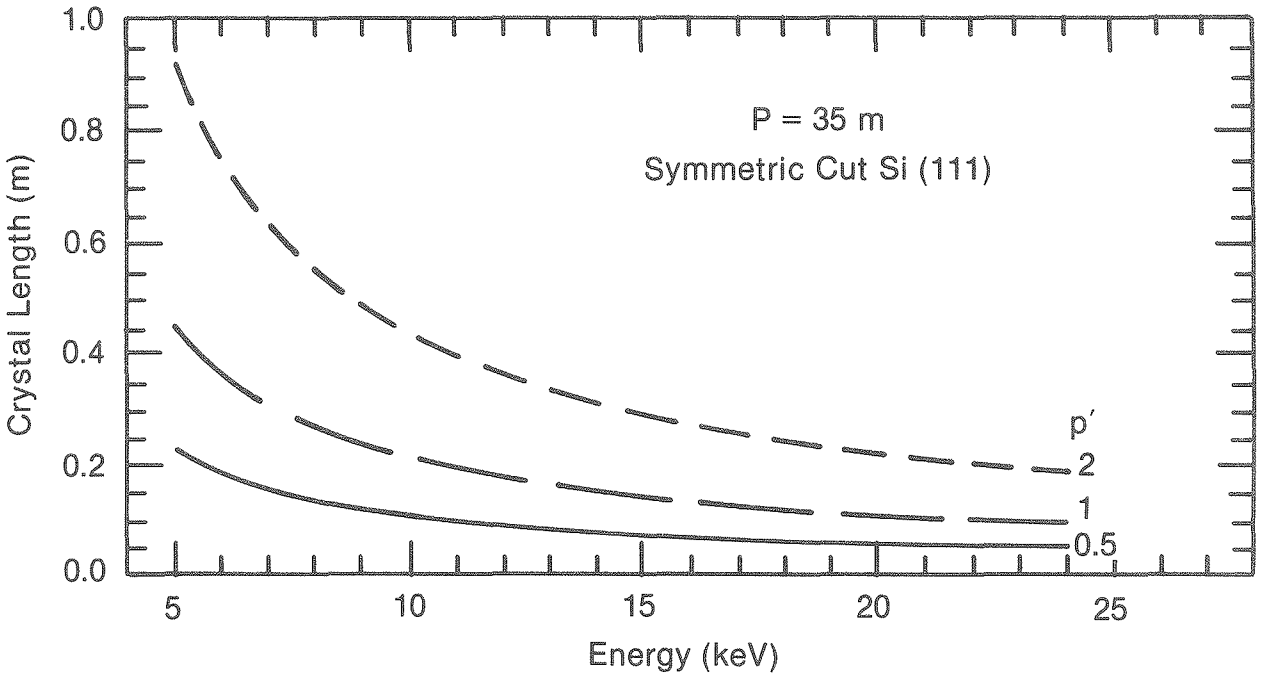

Fig. 11-4 Lengths of crystal footprints for Si(111) crystals with various values of P'

protects ring vacuum and simplifies experimental set-ups. Pre-monochromator beam-defining slits (horizontal and vertical) further reduce total heat load on the crystal and help minimize aberrations; post-monochromator slits and shutters better define the beam and allow manipulation of experimental equipment while allowing the crystal to maintain thermal equilibrium between periods of data acquisition.

Significant development of position-sensitive detectors is necessary to produce a system capable of handling high count rates over a broad dynamic range. This development is currently under way at Argonne. For both condensed matter and gas phase experiments at high spatial resolution, beam-defining apertures are necessary. These apertures should cover a range of sizes (0.5-50 μm) and must be reliably positioned either along or perpendicular to the focused beam axis. Consequently, both encoding devices and microscopic (SEM or optical) visual inspection are necessary for alignment. Sample positioning for solid materials also needs a high degree of spatial reproducibility, which can be achieved by effectively using the technology currently employed in electron microscopy. This entire experimental "back end" can be removed easily for working in the time-resolved mode.

REFERENCE

1. G. K. Shenoy and P. J. Viccaro, "An Overview of the Characteristics of the 6 GeV Synchrotron Radiation: A Preliminary Guide for Users," ANL Report ANL-85-69 (October 1985).

12 Medical Diagnostic Beamline

12.1 Coronary Angiography: Background and Justification

Over 600,000 people die each year in the United States from myocardial infarction (heart attack); it is the leading cause of death in this country. Half of these people die without prior knowledge of their illness. Economically, heart disease is the most expensive health problem in the nation, in terms of both clinical treatment and the loss to society of the creative, active, productive, and trained people. A safe screening method to test everyone for heart disease would be among the greatest public health advances of the century, since many effective methods now exist to treat heart disease if it is recognized.

Currently, the only truly effective method to determine the extent of coronary vascular disease is the coronary angiogram. Coronary angiography, when performed in a specialty center by competent specialists, is generally safe. However, it is expensive and requires highly trained teams of physicians and technicians. Furthermore, when performed outside a specialty center, it is associated with a nontrivial risk. About 1% of all patients who undergo coronary angiography suffer some major complication of the procedure: death or a non-fatal sequel such as a stroke or heart attack. Such complications are a consequence of the invasive nature of this procedure: a stiff plastic tube is inserted into the coronary arteries through the aorta. Coronary angiography is essential prior to any cardiac surgical intervention, and it is the definitive method to characterize the state of a patient's coronary vasculature. But it is too expensive and too inherently risky to be used as a routine screening examination.

A research group at SSRL has performed feasibility studies suggesting that synchrotron radiation can be used to create a safe screening

angiography technique that exposes patients to low radiation doses, involves no risky invasive procedures, is inherently inexpensive (if performed en masse), and has sufficient spatial resolution to allow visualization of small arterial defects.

We propose a coronary angiography procedure based on the initial studies at Stanford. The principal feature that distinguishes our system is that our imaging method, to be implemented on the 6 GeV Light Source, is a 2-dimensional one, whereas all previous studies have used linear imaging with linear detectors. Two-dimensional imaging allows real-time stop-action studies of the coronary arteries, and the images therefore do not have motion artifacts, which are a feature of linear imaging. We believe that this imaging capability, and the special design features of our apparatus, can make coronary angiography on the 6 GeV Light Source a high-quality, safe, and easily used procedure that will be compatible with public health screening of the general populace for coronary vascular disease. Such 2-dimensional imaging is only possible with the very high x-ray flux that can be achieved with the 6 GeV Light Source.

12.2 Description of the Technique

12.2.1 Introduction

This technique exploits iodine's K absorption edge at 33 keV. As with conventional arteriography, iodine is introduced into the blood and is observed within the arteries so that their quality can be visualized. On the synchrotron, the iodine is introduced through an arm vein; this procedure is safe, easy, and noninvasive. Two images are recorded: one just above and one just below the iodine K-edge. Since the linear absorption coefficient of iodine changes from 36 cm^2/g to 6 cm^2/g across this edge and no other body

constituent shows a comparable change, only iodine can be visualized after digital subtraction of the two images (the actual enhancement of iodine relative to soft tissues is 143,000-fold).

12.2.2 The Contrast Agent and Its Introduction into the Patient

The contrast agent is cardiografin, an organically bound form of iodine (Squibb Corp.; chemical name diatrizoate meglumine; an aqueous solution containing 40 g iodine/100 ml). A bolus of cardiografin (0.75 ml/kg in 1 sec) is introduced intravenously through the antecubital vein. After about 4 sec, this bolus, diluted about 10-fold, enters the left cardiac ventricle and cardiografin begins to fill the coronary arteries via the aorta. At a blood iodine concentration of 40 mg/cm^3, the difference in absorption coefficient for the two photon beams is 1.2/cm, so a 0.25-mm feature in an artery would give a 3% change in linear absorption across the iodine K-edge by 5 seconds after administration of the contrast agent.

12.2.3 Absorption of Radiation by the Whole Body: Signal Attenuation

At 33 keV, the linear x-ray absorption coefficient of human tissue is ~ 0.33/cm, which is indistinguishable from that of water. In passing through the body, the x-ray beam must penetrate about 19 cm of tissue, so $I/I_o = \exp(-6.2) = 0.002$; i.e., the beam is attenuated by a factor of ~ 500.

12.2.4 Counting Rates, Sensitivity, and Exposure Times

We need to record the image of the coronary arteries, which are moving rapidly, in a time period that is short with respect to the cardiac cycle period of about 400 msec; we aim for a 20-msec exposure time. The area to be imaged is about 15 cm x 15 cm, and we aim for a 0.25-mm spatial

resolution, so we need 600 x 600 = 3.6×10^5 pixels. To detect a 3% signal (see above) with a 1:1 signal-to-noise ratio, we must reduce all errors (statistical and systematic) to a 3% level. If we conservatively assume a 4-fold loss of signal due to detector noise, signal loss, and other factors, we need 4.4×10^3 counts per pixel or 1.6×10^9 counts over the entire detector surface. Allowing for the 500-fold attenuation through the patient, we require 1.6×10^{12} photons (both beams) impinging on the patient in 0.02 sec, or a flux of 8×10^{13} photons/sec (both beams) from the wiggler source. These figures are summarized in Table 12-1.

12.2.5 Patient Exposure Doses: Safety

One rad equals 6.242×10^{10} keV/g of tissue, or 1.9×10^9 photons/g at 33 keV. The photon deposition per centimeter of penetration is $0.33\ I_o \exp(-0.33\ d)$. Therefore, during the exposure, I_o equals 3.6×10^{11} photons/cm^2/sec, or 7.2×10^9 photons/cm^2. The radiation exposure R as a function of depth d is therefore

$$R = 2.4 \exp(-0.33\ d) \text{ rad.}$$

The radiation exposure of the front skin is therefore about 2.4 rad, that of the heart is about 0.10 rad, and the mean radiation dose is about 0.4 rad. These numbers are very low in comparison to other medical procedures; for example, a typical chest x-ray gives an exposure of about 1.0 rad, and patients undergoing conventional coronary angiography receive

Table 12-1

Summary of Statistical Analysis of the Medical Diagnostic Beamline

Number of pixels	$600 \times 600 = 3.6 \times 10^5$
Size of each pixel (mm)	0.25 x 0.25
Physical size of detector array (cm)	15 x 15
Photon flux (photons/sec/0.1%BW/mrad θ) at 33 keV	8.0×10^{14}
Fraction of Gaussian distribution of the photon beam in vertical direction that is projected onto the radiography stage by both beams	76%
Fraction of hyperbolic distribution of the photon beam in horizontal direction that is projected onto the radiography stage (mrad θ) (0.67 of full 2-mrad dist.)	1.0
Fraction of 0.1% BW diffracted by bent crystals	50%
Reflection coefficient of bent Si crystals	0.95
FWHM rocking curve for bent crystals (arc sec)	6.0
Transmission through the patient's body	$\exp(-6.2) = 2 \times 10^{-3}$
Change in absorption coefficient ("signal strength") across iodine K-edge for 0.25-mm artery	3%
Length of simultaneous exposure to both wavelengths (msec)	20
Flux on front of patient in 20 msec (photons per beam)	2.9×10^{12}
Flux on patient per pixel in 20 msec (photons per beam)	8×10^6
Flux on detector per pixel in 20 msec	1.6×10^4
Counting statistics, assuming 50% quantum efficiency	1.6%
Signal-to-noise ratio	2:1
Signal-to-noise ratio, assuming 25% quantum efficiency in detectors	1.3:1

doses of 100-300 rad. Doses of 2,000 rad are used in radiotherapy to kill cancer cells.

12.3 Description of the Beamline

The beamline will be a two-wavelength x-ray radiographic instrument capable of taking stop-action radiograms of moving objects (such as a heart) with msec time resolution. A schematic of the beamline is shown in Fig. 12-1. The photon beam is generated by a wiggler insertion device, whose characteristics are defined in Table 12-2 and illustrated in Fig. 12-2. This high-power, high-energy wiggler (total power 16 kW; critical energy 28.7 keV) has a very high peak flux of 8×10^{13} photons/sec/0.1%BW/mrad θ at the iodine K-edge, 33 keV. As shown in Fig. 12-1, the photon beam produced by the wiggler passes out of the experimental hall surrounding the storage ring and enters the special medical building. Here it impinges on two bent crystals which produce radiation at energies above and below the iodine K-edge, respectively. The two crystals not only select the two wavelengths but also (by virtue of their bends) spread the beam vertically; the horizontal spread is due to the wiggler's own characteristics. Two detectors are mounted in a separate building (at the far right of Fig. 12-1) so that they are somewhat above the angiography stage and 75 m downstream; at this distance, beams with different wavelengths will have separated. These two detectors record, respectively, the high- and low-energy beams that passed through the patient.

A second facility, with its own stage and set of detectors, can be set up on the same beamline by mounting a second set of bent crystals about 10 m downstream from the first set. As shown in Fig. 12-1, the second set is oriented so as to diffract the x-ray beam downward instead of upward. The second angiography stage is located one floor below the first stage, and the

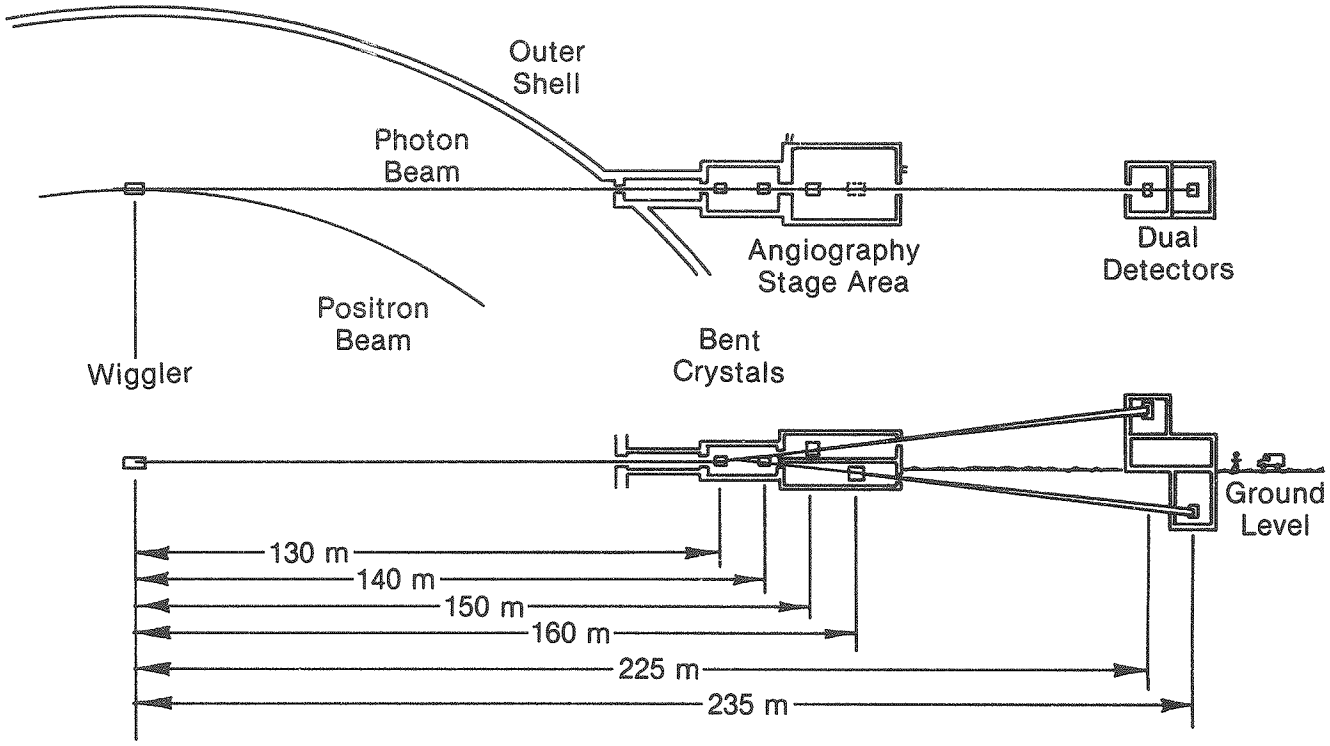

Fig. 12-1 Top and side views of medical diagnostic beamline for the 6 GeV Light Source

Table 12-2

Parameters of the REC Hybrid Wiggler for the Medical Diagnostic Beamline

Magnet Gap (cm)	2.0
Period, λ_o (cm)	10.5
B_o (T) 1.2	
Radius, ρ_o (m)	16.6
K	11.08
No. of Poles, N	94
Length, L (m)	4.935
Critical Energy, E_c (keV)	28.7
Total Power (kW)	16.2
Width of Distribution in Vertical Direction (2ψ mrad)	0.2
Width of Distribution in Horizontal Direction (2θ mrad)	2.0
Peak Power (kW/mrad θ)	10.5
Peak Power (kW/mrad^2)	78.6
Power at Normal Incidence at 20 m (W/mm^2)	196.6
Flux at E_c (ph/sec/0.1%BW/mrad θ)	9×10^{14}
Gap Variability	None

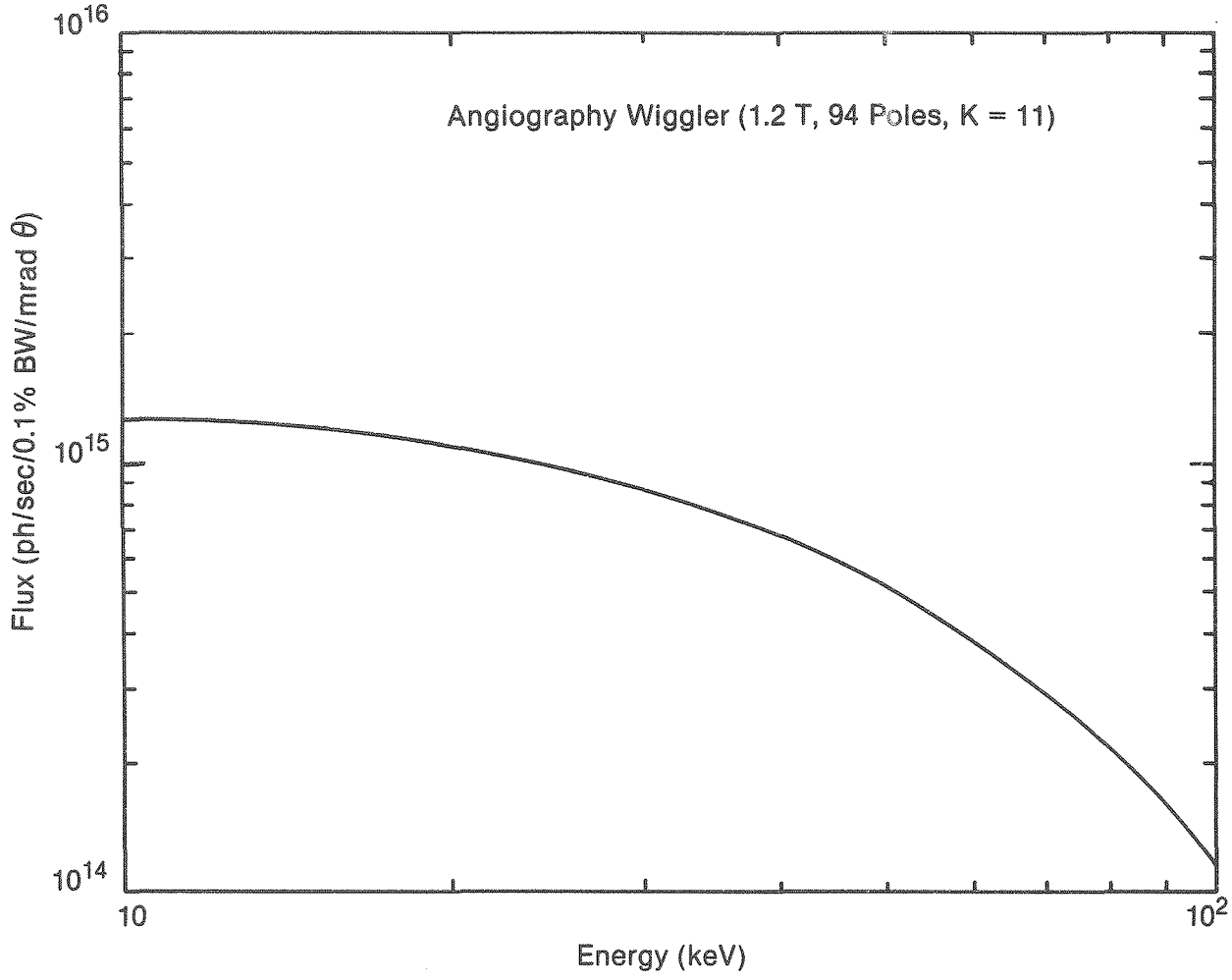

Fig. 12-2 Plot of photon flux vs photon energy for the special angiography wiggler

detectors are in the sub-basement of the detector building. With such an arrangement, one stage can operate while the other is being set up or serviced. One simply lowers the first set of crystals out of the beam so that the second set can be illuminated.

A schematic for the two-wavelength camera for x-ray radiography is shown in Fig. 12-3. The photon beam from the wiggler enters from the left. The first bent crystal intercepts the lower half of this beam. This bent crystal simultaneously selects the wavelength region just above the absorption edge of iodine and spreads this diffracted beam out over the full area of the angiography stage. The second bent crystal intercepts the upper half of the photon beam, selects the wavelength region just below the absorption edge of iodine, and spreads this part of the beam uniformly over the stage.

The x-ray image is recorded by a dual detector assembly which can be two multi-element electronic arrays or two sheets of special x-ray film. As mentioned earlier, it is necessary for the detectors to be a long distance (75 m) from the stage area to obtain complete separation of the two images, because the angle between the two beams is quite small. This distance could be reduced by increasing the angle between the two beams, but this would move the two wavelength regions farther apart in energy and reduce the sensitivity of the experiment by reducing the difference between the absorption coefficients for the two beams.

The curvature of each bent crystal is not constant along its surface, but rather changes smoothly from one end to the other in the direction of the beam. This is done so that the photon flux at the viewing stage is uniform. If the radius of curvature of the crystal were constant, then the upper part of the viewing stage would receive twice as many photons per square centimeter as the bottom part. This is because the beam intensity

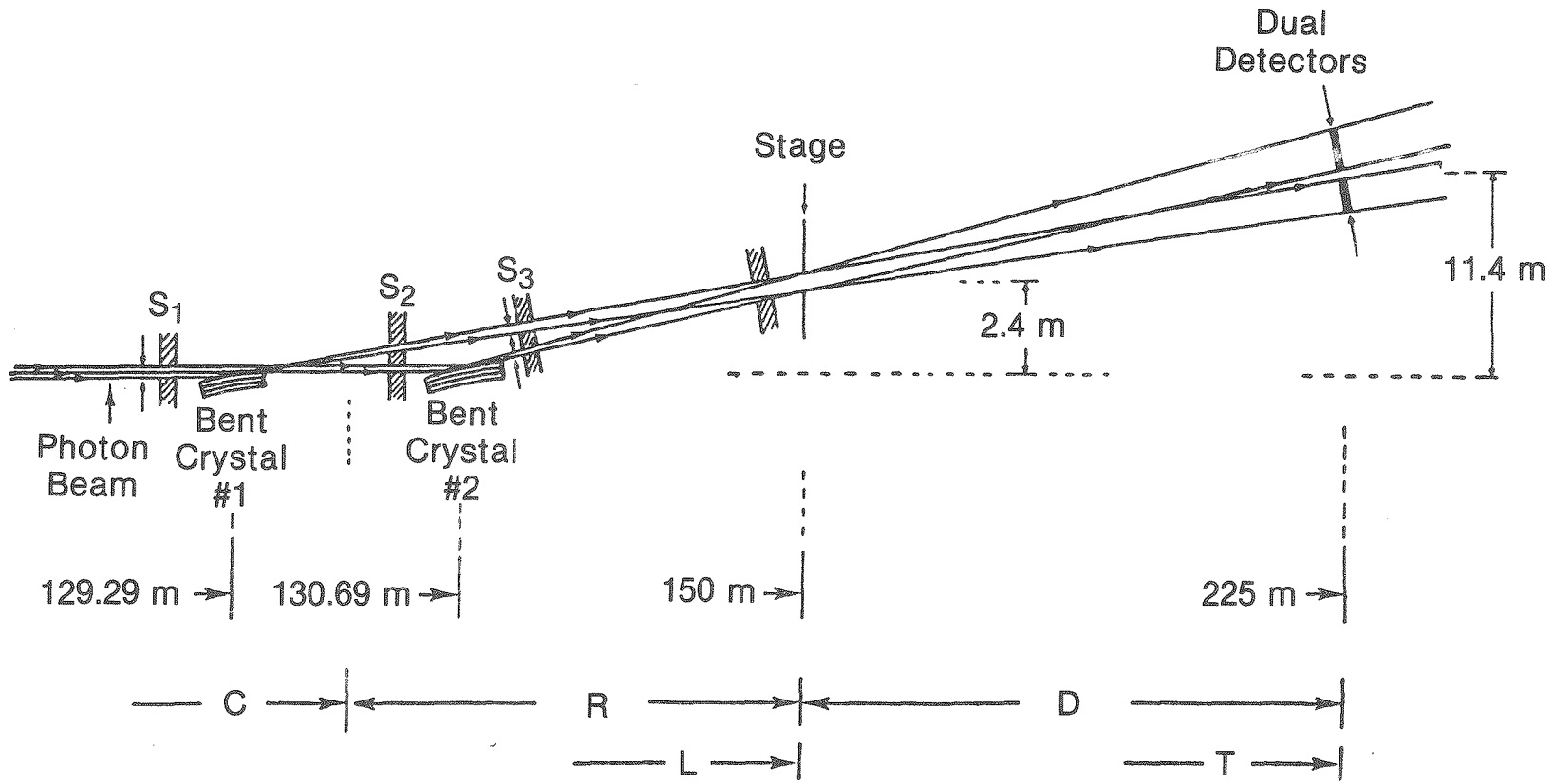

Fig. 12-3 Schematic drawing of the x-ray optical component for a two-wavelength x-ray radiographic instrument capable of taking stop-action radiograms of moving objects such as the heart with msec time resolution

has a Gaussian shape in the vertical direction and the first crystal intercepts the lower half of the beam from the half-height to the peak height position. The reverse is true for the second bent crystal, which intercepts the upper half of the beam from peak to half intensity. Thus the relative intensity of the two beams of different wavelengths would change by a factor of four over the vertical length of the stage. This could be compensated for by normalizing the observed picture intensities as a function of position, but this type of major normalization can introduce error into the subtraction process unless it is very accurately done.

Another reason for having a nonuniform bend is to stabilize the shape of the crystal under the large heat load that is introduced by the beam. If the crystal is bent over a perfect cylinder shape, then the crystalline plate is in dynamic balance and requires no first-order forces on either its underside or its upper surface to make it conform to a cylindrical shape. Only small secondary forces are present to give it slight contact with the surface. All of the first-order bending forces are concentrated near the ends of the crystal. If the radius is changed smoothly along the surface, then the bending forces are distributed over the whole surface of the crystal and a substantial force acts to make the crystal plate conform to the surface of the support plate. This stabilizes the shape of the crystal until the thermal stress exceeds the bending stress.

The characteristics of these two crystals are listed in Table 12-3 along with other important parameters. Note that both a minimum and a maximum crystal radius are given. The terms used in the tables, figures, and discussion are defined in Table 12-4.

Table 12-3

Parameters of the Medical Diagnostic Beamline at the Four Crystal Positions

	First Stage (L = 150 m)		Second Stage (L = 160 m)	
	Crystal 1	Crystal 2	Crystal 1	Crystal 2
Energy (keV)	34.394	31.990	34.394	31.990
θ (deg)	3.301	3.543	3.301	3.543
C (m)	129.29	130.69	139.29	140.69
R (m)	20.71	19.31	20.71	19.31
D (m)	75.0	75.0	75.0	75.0
Δy (cm)	1.29	1.31	1.39	1.41
Δx (cm)	12.95	13.05	13.95	14.05
Δz (cm)	10.86	10.95	11.68	11.80
Δb (mrad)	3.328	3.547	3.283	3.521
Δb' (mrad)	3.228	3.447	3.183	3.421
ΔE (keV)	1.961	1.730	1.896	1.821
Peak Power (W/cm^2)	14.2	14.2	9.4	9.4
ΔT(C)/cm (°C/cm)	10.9	10.9	7.2	7.2
Minimum Crystal Radius (m)	52.0	50.1	55.8	52.4
Maximum Crystal Radius (m)	104.1	100.2	111.6	104.9
Thermal Radius (m)	381	381	578	578
Stage Height[a] (m)	2.4	2.4	-2.4	-2.4
Detector Height[a] (m)	11.1	11.7	-11.1	-11.7

[a]Relative to primary beam.

Table 12-4

Definition of Terms and Symbols

θ	angle between photon beam and bent crystal
C	distance from wiggler to center of bent crystal
R	horizontal distance from bent crystal to stage
D	horizontal distance from stage to detector
L	horizontal distance from wiggler to stage
T	horizontal distance from wiggler to detector
Δy	width (FWHM) of photon beam in vertical plane (beam has a Gaussian shape in the vertical direction)
Δx	horizontal width of collimated photon beam on bent crystal
Δz	length of photon beam on bent crystal in the direction of the beam
Δb	angular width of photon beam after it is spread in the vertical direction by the bent crystal
$\Delta b'$	change in angular width in vertical direction generated by bent crystal
ΔE	energy bandwidth of diffracted photon beam
$\Delta T(C)/cm$	thermal gradient perpendicular to surface of bent crystal at point of peak power load
Thermal Radius	radius of curvature in one dimension generated by $\Delta T(C)/cm$ in a uniform crystal plate (a measure of the thermal stress generated in the crystal)

12.4 Flux from Wiggler Source

The estimated peak flux at 33 keV for the wiggler is 8×10^{14} photons/sec/0.1%BW/mrad θ, where θ is the horizontal opening angle. If we assume a 6-arc-sec rocking curve for the Si crystal using the (111) planes, and we assume a 95% reflectivity, the total flux on the angiography stage (15 cm x 15 cm) is 1.44×10^{14} photons/sec. Since we required at least 8×10^{13} photons/sec for adequate counting statistics with 0.25-mm spatial resolution, we are well within our requirements here, especially since we have assumed that we can detect only 25% of the signal. Thus this facility will probably operate effectively even if the synchrotron is not near full power. We can compensate for low output power of the synchrotron by decreasing the effective spatial resolution of the detector. For example, decreasing the resolution to 0.5 mm gives us a factor of 2 increase of the signal-to-noise ratio, so we could operate with this spatial resolution even if the beam intensity dropped by a factor of 4 because of low beam current or imperfect beam optics. This assumes that the objective is to detect 0.25-mm-thick blood vessels. If the detection goal is reduced to blood vessels that are 0.5 mm in diameter, then the system can operate with beam currents of only 1/16 of the 100-mA design current, i.e., 6 mA.

12.5 Stability

Each arm of the two-wavelength camera contains only one optical element, a bent crystal. This greatly simplifies the design and eliminates almost all of the normally critical alignments and precision locations for the x-ray optics. The large bandwidth used in each projected beam eliminates the rest of the critical alignments. It also eliminates the need to maintain any critical alignments between the positron beam in the accelerator and the

crystals in the beamline. The positron beam could move up and down or sideways by 1 mm, without noticeably affecting the performance of the system. Variations in the beam intensity are automatically normalized to first order by the simultaneous acquisition of data in both detectors. Thus, even large (factor of two) changes in beam intensity will require only modest normalization corrections. This insensitivity to component alignment makes it possible to consider systems with more than one viewing stage.

12.6 Summary of Special Features

A summary of the medical beamline parameters as given in Table 12-1. The special features of this facility include:

1. Capability for visualizing a selected element.
2. Simplicity, with only one optical component per diffracted photon beam.
3. Elimination of any requirement for critical alignments between the optical components, or between them and the beamline or the positron beam.
4. Good statistics, with short exposures possible because of the high photon flux.
5. Good normalization between the two images due to simultaneous detection of both photon beams.
6. Very low exposure of patient to radiation (comparable to a routine chest x-ray).
7. High degree of safety for patient relative to the high-risk procedures used in conventional angiography.

13 Transuranium Research Facility

13.1 Introduction

A heavy user demand for beam time for transuranium research is anticipated at the 6 GeV Light Source. Argonne has a long-standing safety record in handling large quantities of transuranics. In addition, an outstanding facility for producing, characterizing, and handling transuranium systems has been developed in the Materials Science and Technology Division. Finally, Argonne has taken the lead in building a prototype transuranium beamline at the U-2 port of the NSLS. With this experience and background in the area of transuranium materials, Argonne scientists can provide the leadership and guidance needed to build a transuranium facility at the 6 GeV Light Source.

Many new solid-state phenomena such as narrow-band magnetism and superconductivity, heavy fermions, and strongly interacting Kondo systems manifest themselves in the hybrized 5-f orbitals of transuranium systems. Sufficient quantities of materials are now available to allow preparation and characterization of systems of transuranics up to californium. Thus, the unusual properties of these new systems are expected to attract the interest of many investigators in the new future. The high-brilliance 6 GeV Light Source will provide many unusual techniques for their study.

13.2 Transuranium Beamline

In general, transuranium studies with hard x-rays (above 5 keV) pose no contamination problem, since the use of a window allows the safe confinement of transuranium samples away from the ring. Problems are encountered primarily in dealing with soft x-rays (VUV), where it is necessary to have the experimental chamber exposed to the ring vacuum. Still, since the

handling of transuranic materials for both x-ray and VUV research requires the same precautions (a hutch with a filtered air intake and exhaust, gloveboxes, and associated radioactive handling facilities), it is wise to consider providing both x-ray and VUV capability on the same beamline, by using a mirror to deflect part of a low-E_c wiggler beam. It should be pointed out that the term "transuranium beamline" actually refers only to a transuranium spectrometer, since it is essential that the beamline itself remain uncontaminated at all times.

Figure 13-1 schematically depicts the layout of a transuranium beamline. A sealed hutch encloses both the VUV and x-ray spectrometers. The hutch is maintained at a slight underpressure via a fan and a pressure controller on the filtered exhaust side of the hutch. This prevents particles from diffusing into the large experimental area in case of small spills while loading and unloading samples.

The beam deflector, as presently envisioned, is a movable, cooled, platinum-coated mirror, approximately 1 m long, positioned at 2° grazing incidence about 30 m from the source. A mirror of this size will accommodate a beam with 1 mrad of divergence, and will reflect it at a 4° angle. The mirror will be removed for x-ray experiments.

Although safety considerations are expected to preclude simultaneous operation of the VUV and x-ray lines, the present design allows for simultaneous operation by positioning of the mirror to intersect only part of the beam. For higher intensities, the entire beam will need to be subtended.

A grating monochromator (possibly a plane-grating UMO-type) will be used on the VUV line, and a double-crystal monochromator together with a premonochromator will be used on the x-ray line. If a UMO plane-grating

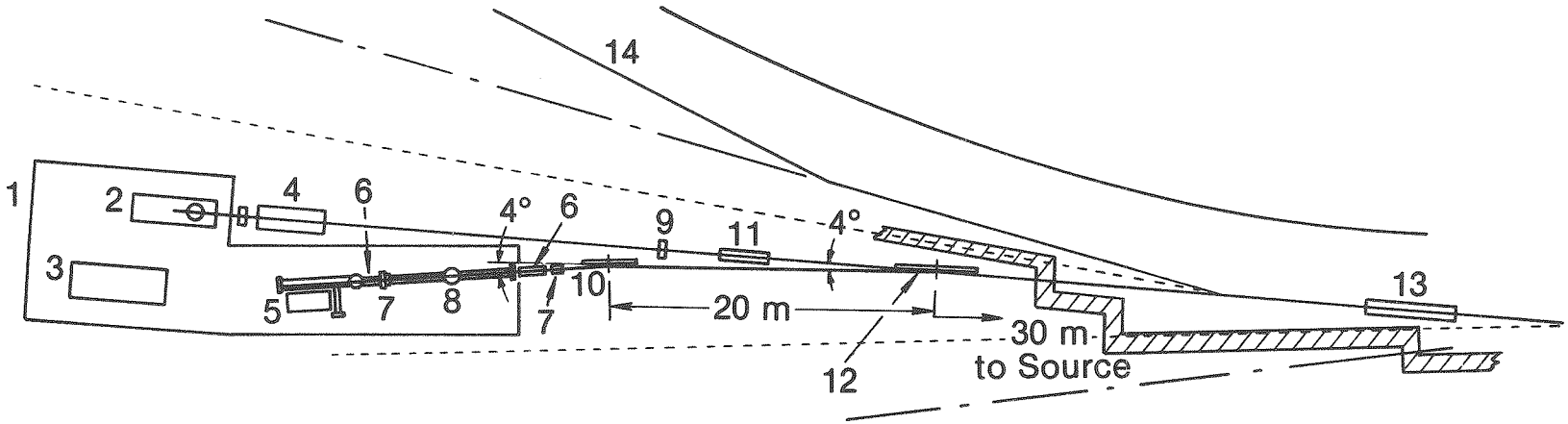

1. Hutch
2. X-Ray Experimental Station
3. Repair and Storage Glovebox
4. Crystal Monochromator
5. UV Experimental Station
6. Delay Line
7. Fast Valve
8. Grating Monochromator
9. Be-Window
10. Focusing Mirror
11. Pre-Monochromator
12. Cooled Plane Mirror
13. Source
14. Ring

Fig. 13-1 Schematic layout of the transuranium area

monochromator is used, it may be helpful to use a bent cylindrical mirror to deflect the low-energy beam and reflect parallel rays; this will allow the monochromator to be placed at a large distance. Because of the need for frequent access to the VUV monochromator, it will be placed inside the hutch. An added benefit is that this allows one to do experiments that pose a greater contamination risk, since the monochromator can sustain mild contamination if kept in a closed environment.

Since a beryllium window will separate the x-ray monochromator from the x-ray experimental area, the x-ray portions of the hutch will be relatively simple, consisting only of an experimental station enclosed in a glovebox. Only the normal sample-handling precautions used in the laboratory need be considered here, since the chances of ring contamination are minimal.

The VUV station, however, requires special consideration since up to now no suitable window material has been found which transmits adequately in the 10-eV to 1000-eV range. The necessary precautions do not change dramatically even if a window material is found, since it is likely to be a thin membrane subject to a large stress. The intense radioactivity of these materials necessitates special precautions to safeguard the ring and ring area from possible contamination. Hence, users of such a beamline facility will be expected to follow the Argonne philosophy of safety when handling transuranics. This philosophy has the following important ingredients: (1) User training in operating the materials facility and the beamline, (2) strict materials inventory at every stage of sample handling, (3) frequent monitoring during the use of the beamline, (4) double containment of samples, and (5) double contingency in accident analysis.

Figure 13-2 shows a schematic layout of the VUV transuranium experimental area. The spectrometer chamber will be open to the beamline and

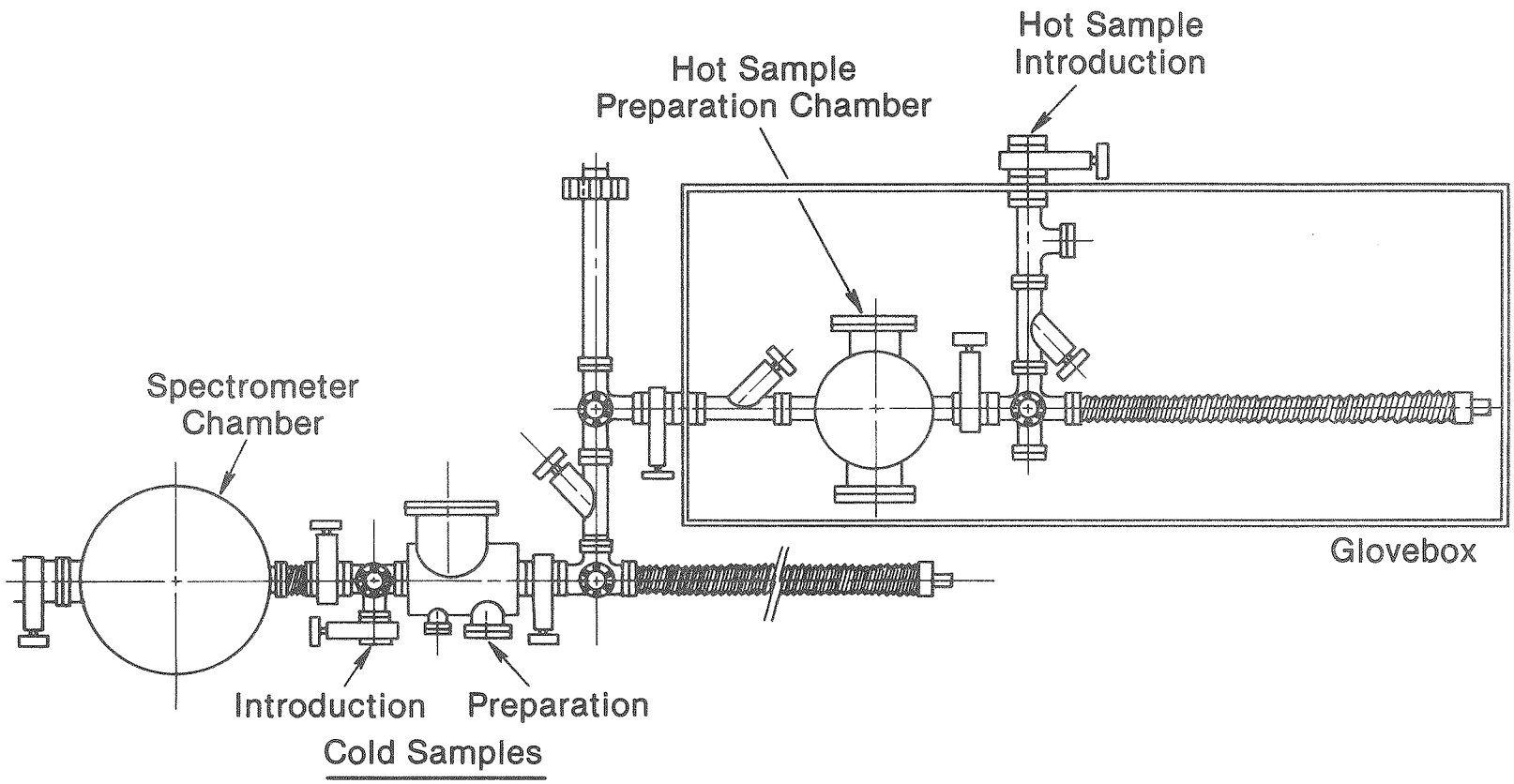

Fig. 13-2 Schematic layout of the VUV transuranium experimental area

hence must remain "cold" even though "hot" samples are introduced for measurement. This is accomplished by having a second "hot" sample preparation chamber enclosed in a glovebox in which all surface preparation is carried out. A cleaned (prepared) sample is then transferred via a tortuous route into the "clean" spectrometer chamber. The general philosophy is as follows:

1. All operations that remove material are done in the "hot" preparation chamber. These include sputtering, cleaning, heating, scraping, and evaporating.

2. The amount of material in all experimental chambers is kept to a minimum at all times (i.e., no long-term storage of samples).

3. A tortuous transfer route is used to prevent diffusion of microscopic particles into the spectrometer chamber.

4. Interlocks are used to prevent the simultaneous opening of the beamline and any portion of the preparation chamber or transfer route.

5. Measures are taken to protect the ring in case of catastrophic vacuum loss in the chamber:

   - To prevent macroscopic particles from entering the beamline, the slit that admits light to spectrometer chamber is made small.
   - A delay line immediately downstream from the chamber gives all fast-actuating valves time to close.
   - Additional fast-acting valves are placed, just upstream of the delay line that leads to the monochromator.

- Since windows are the most likely source of catastrophic vacuum loss, plexiglass covers are placed over all windows to reduce the probability of such an occurrence.

6. Radiation levels in the spectrometer chamber and beamline are frequently monitored. If levels exceed 10^4 dpm, the chamber is cleaned.

7. The following categories of transuranics are not allowed in the spectrometer chamber:

   - powders
   - gas phases
   - unstable materials

8. Strict adherence to operating procedures is required.

14 Beamline Computer Systems

14.1 Introduction

To guarantee adequate real-time response for time-critical experiments, each beamline should have its own dedicated computer for process control and data acquisition. This computer should be powerful and flexible enough to readily accommodate itself to most conceivable experimental needs, although there will be instances in which experimenters will need or want to use their own computer systems. D/A modules and digital control units are used to set experimental parameters such as temperature and gas pressure. The data are typically acquired through the use of A/D modules and counters, although the requirements of the individual experiment may dictate the use of special-purpose units such as those available in the CAMAC architecture, dedicated special-purpose backplane boards, and specialized units such as multichannel analyzers, which are connected to the computer via a standard interface such as IEEE-488.

The selection and setup of the hardware requires considerable knowledge and effort. Typically, the hardware and software development for an experiment constitutes more than half the total effort involved in the operation of a beamline. Often, poor initial choices result in the need for substantial hardware changes or frequent modifications of the software during the course of the experiment. Consequently, there is sometimes significant financial waste and, more importantly, loss of usable beam time.

To the extent that the needs of the experiments permit, standardized (or at least compatible) computer equipment should be used on all the beamlines. This policy permits the rapid interchange of components or complete computer systems, both for fault detection and repair, and the rapid reconfiguration of a beamline for different experiments. This policy also

makes it possible for the laboratory to provide in-house support in the form of standardized modules, e.g., stepping motor controls, and a resource pool for itinerant users. In this way, it should be possible to substantially improve the productivity of the beamline users. A generic Digital Equipment Corp. (DEC) LSI-11-based process control system, "SCAMP", has been developed at Argonne for use with experiments being performed on the ATLAS accelerator. SCAMP provides a process control and data acquisition framework into which the user's application can be linked. The adaptation and extension of SCAMP to the needs of 6 GeV Light Source users would be a major priority of the support group.

In order to facilitate program development, the beamline computers, or their equivalents, should be accessible to off-site experimenters prior to their arrival at Argonne. This access could be either local, by use of a comparable machine at the user's institution, or remote, through access to a development machine at Argonne. Equivalence to the beamline computer can mean either that the development computer is a similar machine or that it is capable of emulating the dedicated beamline computer.

Although a dedicated microcomputer is highly desirable for process control and data acquisition, it may not be the best choice for data analysis. Consequently, for cases when extensive data reduction is required to monitor the course of an experiment, there will be a high-speed data link to a central "super"-minicomputer, described in the proposal for the 6 GeV Light Source. In this section, the term "6 GeV central computer" will refer to this super-minicomputer rather than to the similar machine used by the Light Source operators to control the operation of the synchrotron. The 6 GeV central computer will also in many cases be the machine of choice for postexperiment data analysis. To handle experiments that require massive

number crunching, a link will be provided between the 6 GeV central computer and Argonne's CRAY-class supercomputer.

The schematic of Fig. 14-1 shows the relationship between the dedicated MicroVAX II beamline computers, the 6 GeV central computer, and the Argonne supercomputer.

14.2 Summary of Beamline Users' Computer Needs

1. Each beamline will have a dedicated computer for experiment control and data acquisition.

2. Beamline computers will be standardized but flexible enough to satisfy the needs of most users. It should be possible to reconfigure them for difficult experiments with a minimum of downtime. Users will use their own computers only when they have special needs beyond the capabilities of the standard machines. This arrangement will facilitate (a) on-site support and repair, (b) standardization of software and hardware modules, and (c) on-site debugging of software.

3. Off-site program development requires that equivalent computers be readily available throughout the country, or that the standard beamline computers be software-compatible with a readily available computer.

4. There will be a high-speed data link for transfer of data from the beamline computers to a central computer for data processing.

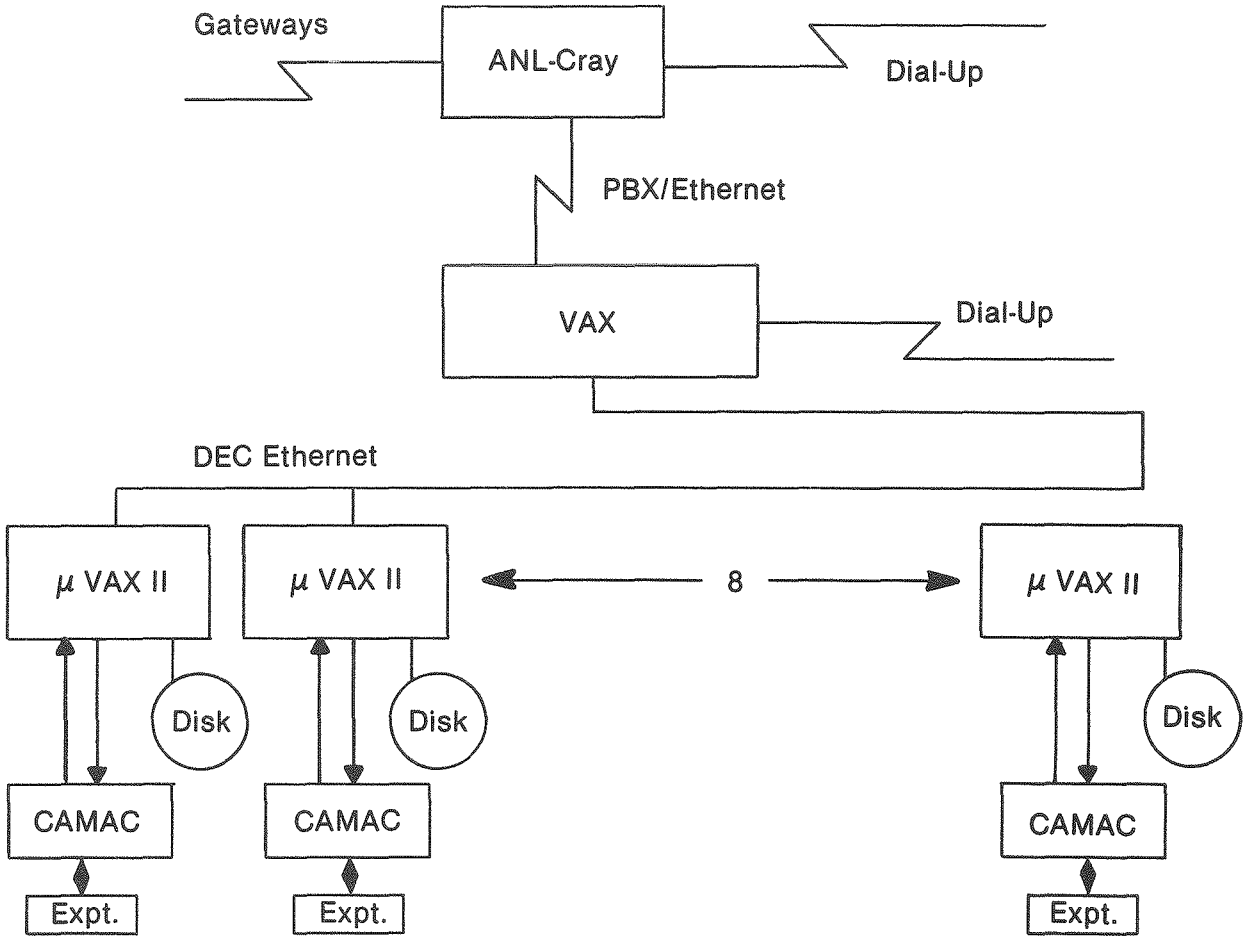

6-GeV Beamline Control/Data Acquisition Computer System

Fig. 14-1 Computer system for experimental process control and data acquisition at the 6 GeV Light Source. Each of the beamlines has a dedicated MicroVAX II.

5. Both soft- and hard-copy graphics of raw and partially reduced data will be available at the beamline computer for monitoring the progress of an experiment. Graphics at the beamline need not be of publication quality, but high-quality graphics will be available through the central facility.

6. Ultimate responsibility for beamline interfacing must lie with the experimenters. However, a standard interface that will be adequate for most experiments will be provided with the front-end computers. Hardware and software support for the standard configurations will be provided by the 6 GeV Light Source staff. The support staff will also develop more specialized interfaces on a cost-recovery basis. Because of the range of possible experiments, extraordinary process control and data acquisition costs must be borne by the individual experiments.

14.3 Implementation

This section presents recommendations for the system configuration, based on systems currently or shortly to be available. Since computer hardware is undergoing rapid change and the system will not be installed for several years, these recommendations are at best provisional.

14.3.1 Hardware/Software

We recommend that DEC MicroVAX II (or III) computers running under either the VMS or the VAXeLan operating system be used as front-end computers for the following reasons:

1. There is currently substantial expertise available at Argonne in the use of DEC LSI-11 and PDP-11 microcomputers for dedicated experiment control and data acquisition. Additionally, the larger VAX machines are widely used at the laboratory for data reduction, and substantial capabilities for file transfer between VAX and smaller DEC machines are available. Special interfaces similar to those available for the DEC LSI-11 and PDP-11 series computers are rapidly becoming available for the MicroVAX. These interfaces make it very easy to add additional control and data acquisition capability.

2. Large amounts of additional memory and disk capacity can be easily added to meet users' needs. The MicroVAX supports a very large (16-Mbyte) linear address space. Up to this limit, additional memory can be added transparently, i.e., without modifying either the operating system or the application software. Since memory paging is not required to address a large memory space, the MicroVAX is capable of storing and retrieving large amounts of data much faster than a computer employing paged memory. For applications requiring extremely large on-line capacity, groups of MicroVAX IIIs (to be released in early 1986) can be connected in tandem.

3. The MicroVAX series machine, running under the VMS operating system, is fully software-compatible with the widely available VAX super-minicomputers. If it is necessary for the beamline computer to have multiuser, multitasking capabilities, VMS would be the operating system of choice. Any VAX accessible from the user's home institution can then

be used as a software development machine. Typically, programs written on such systems would be in Fortran.

4. If multiuser, multitasking capabilities are not important for an experiment, the VAXeLan operating system running under VMS or MicroVMS provides a faster response and simplified programming, although programming must be done in C language. Although the larger VAX machines normally run under VMS, the VAXeLan simulator makes it possible to use a VAX as a development machine for the MicroVAX computers.

5. If a VAX is not available at the user's home institution, the VAX super-mini at Argonne can support a number of concurrent remote users for program development via dial-in lines or dedicated networks such as MFENET, TYMNET, or BITNET. Gateways to a number of these networks have already been established from existing VAX machines at Argonne.

14.3.2 Interfacing

It is provisionally recommended that CAMAC (IEEE-583) be used as the standard interface. The CAMAC modules are readily interchangeable, and the CAMAC crate may easily be switched from one computer to another during program development and debugging. For special applications, it may be desirable to use dedicated backplane boards or the GPIB interface. In the former case, CAMAC does not conflict with the use of backplane boards and, in the latter case, a CAMAC-GPIB interface is available.

A reference configuration is shown in Table 14-1. This configuration is capable of providing most of the necessary functions, although some experiments may need more modules of a given type, and a few

will require more powerful computers (e.g., a VAX) or instrumentation not shown in the reference configuration.

Table 14-1

CAMAC Reference Configuration

No. of Units	Item	Kinetic Systems Model #
1	25-station CAMAC crate	1500
1	CAMAC crate controller	3920Z1B
1	CAMAC bus adapter w/DMA	2920Z2B
1	DMA/VMS driver	6610-0BAC
1	Timed output with ac switches	3040A1A
2	16-bit input gate/output register	3061
1	8-channel, 12-bit D/A converter	3112
6	Stepping-motor controller	3361
3	Stepping-motor power supply	5461
1	GPIB interface	3388
1	16-channel, 12-bit A/D converter	3512
1	6-channel, 24-bit, 50-MHz counter	3610
1	4-channel up-down presettable 16-bit counter	3640

14.3.3 Communications

1. Communication and file transfer between the beamlines and the 6-GeV central computer will be via DEC Ethernet. Software modules developed on the VAX can be downloaded through the network to the beamline computers. In addition to its function as the development machine for a specific experiment, the VAX host can be used as a means of distributing standardized modules, or as a means of sharing user-developed special-purpose programs.

2. For data acquisition purposes, VAXeLan offers the choice of either using local disk storage or transferring data to the host computer via Ethernet. DEC Ethernet supports a 10-Mbaud data transfer rate which, for a single machine on the network, is as fast as storage on dedicated hard-disk drives. However, if a number of experiments use the network simultaneously, the transfer rate per user will decrease proportionately. For real-time data acquisition purposes, it will therefore not be possible to use the network to replace local disk storage. However, for preliminary data reduction, it is desirable to off-load the data to the host machine and resume data collection as quickly as possible.

14.3.4 Support

The VAX can be used remotely to serve a number of beamline users during the initial stages of software development. However, the VAX cannot, in its host capacity, drive external process control and data acquisition modules. Final debugging must be done on a machine that is capable of

driving external devices. For this reason, a minimum of two MicroVAX computers will be available for final debugging of experiment software: one running as a remotely accessed multiuser machine under VMS with no external devices, and the other running under VAXeLan with external devices in a single-user mode. Two additional machines should be available for the in-house support staff.